OPEN ACCESS
CellPress

Cell Reports
Article

Endogenous RNAs Modulate MicroRNA Sorting to Exosomes and Transfer to Acceptor Cells

Mario Leonardo Squadrito,[1,4] Caroline Baer,[1,4] Frédéric Burdet,[2] Claudio Maderna,[1] Gregor D. Gilfillan,[3] Robert Lyle,[3] Mark Ibberson,[2] and Michele De Palma[1,*]

[1]Swiss Institute for Experimental Cancer Research (ISREC), School of Life Sciences, École Polytechnique Fédérale de Lausanne (EPFL), 1015 Lausanne, Switzerland

[2]Vital-IT, Swiss Institute of Bioinformatics (SIB), 1015 Lausanne, Switzerland

[3]Department of Medical Genetics and Norwegian High-Throughput Sequencing Centre (NSC), Oslo University Hospital, Kirkeveien 166, 0407 Oslo, Norway

[4]Co-first author

*Correspondence: michele.depalma@epfl.ch

http://dx.doi.org/10.1016/j.celrep.2014.07.035

SUMMARY

MicroRNA (miRNA) transfer via exosomes may mediate cell-to-cell communication. Interestingly, specific miRNAs are enriched in exosomes in a cell-type-dependent fashion. However, the mechanisms whereby miRNAs are sorted to exosomes and the significance of miRNA transfer to acceptor cells are unclear. We used macrophages and endothelial cells (ECs) as a model of heterotypic cell communication in order to investigate both processes. RNA profiling of macrophages and their exosomes shows that miRNA sorting to exosomes is modulated by cell-activation-dependent changes of miRNA target levels in the producer cells. Genetically perturbing the expression of individual miRNAs or their targeted transcripts promotes bidirectional miRNA relocation from the cell cytoplasm/P bodies (sites of miRNA activity) to multivesicular bodies (sites of exosome biogenesis) and controls miRNA sorting to exosomes. Furthermore, the use of *Dicer*-deficient cells and reporter lentiviral vectors (LVs) for miRNA activity shows that exosomal miRNAs are transferred from macrophages to ECs to detectably repress targeted sequences.

INTRODUCTION

MicroRNAs (miRNAs/miRs) are a class of small noncoding RNAs that regulate gene expression at the posttranscriptional level (Yates et al., 2013). Precursor miRNAs are exported from the cell nucleus to the cytoplasm, where they are processed into mature miRNAs by the enzyme DICER. Upon loading into the RNA-induced silencing complex (RISC), miRNAs bind the 3′ UTR of target transcripts to fine-tune their expression via degradation and/or translational repression (Bartel, 2009). Several hundreds of mature miRNAs have been identified in metazoans, many of which are predicted to modulate the expression of multiple gene transcripts (Lewis et al., 2005). miRNAs are also detected in extracellular compartments, such as body fluids, either in complex with proteins of the argonaute (AGO) family or loaded into exosomes (Turchinovich et al., 2012). Exosomes are microvesicles produced by multiple cell types, which originate from the fusion of late endosomes/multivesicular bodies (MVBs) with the cell plasma membrane. Upon their release in the extracellular environment, exosomes can fuse with live cells, either paracrinally or endocrinally, and transfer their cargo of proteins, lipids, and RNAs to the acceptor cells (Simons and Raposo, 2009).

RNA sequencing (RNA-seq) has shown that miRNAs are abundant in exosomes. Notably, the miRNA repertoire of exosomes may differ from that of the producer cell (Gibbings et al., 2009; Guduric-Fuchs et al., 2012; Nolte-'t Hoen et al., 2012; Simons and Raposo, 2009; Skog et al., 2008; Valadi et al., 2007). This finding suggests that the sorting of specific miRNA species to exosomes may be actively regulated, although the underlying mechanisms remain largely unknown. Both the process of MVB/exosome biogenesis and miRNA-sequence-specific determinants may modulate miRNA sorting to exosomes. Members of the endosomal sorting complex required for transport (ESCRT) play crucial functions in MVB biogenesis and exocytosis. However, knockdown of ESCRT proteins does not affect miRNA sorting to exosomes (Kosaka et al., 2010). A recent study identified a specific 4 nt sequence (GGAG) that is overrepresented in miRNAs that are enriched in T cell-derived exosomes. The GGAG motif is bound by sumoylated hnRNPA2B1 (a heterogeneous nuclear riboprotein), which directs miRNA trafficking to MVBs and their secretion via exosomes (Villarroya-Beltri et al., 2013). Thus, specific motifs present in certain miRNAs may guide their sorting to exosomes through the interaction with specific chaperon proteins.

Multiple cell types, such as immune cells, endothelial cells (ECs), and cancer cells, can internalize exosomes secreted by other cells. Several studies have proposed that the transfer of exosomal miRNAs may modulate the biological functions of the acceptor cells (Hergenreider et al., 2012; Mittelbrunn et al., 2011; Montecalvo et al., 2012; Ramachandran and Palanisamy,

2012; Valadi et al., 2007). Nevertheless, distinguishing exogenous miRNA transfer/activity from the endogenous activation of miRNA transcription/activity consequent to exosome-cell physical interactions may prove challenging; therefore, definitive evidence for the robustness of transfer of miRNA activity from exosomes to acceptor cells remains scant. In this study, we employed macrophages and ECs as a model system to investigate the molecular determinants of miRNA sorting to exosomes and transfer to acceptor cells. Our findings indicate that miRNA sorting to exosomes is regulated, at least in part, by cell-activation-dependent changes of targeted transcript levels in the cell cytoplasm. Furthermore, by employing sensitive reporter lentiviral vectors (LVs), we show that transfer of miRNA activity from macrophage-derived exosomes has the potential to detectably modulate the gene expression and biology of acceptor ECs.

RESULTS

Cell-Activation-Dependent miRNA Enrichment in Exosomes

We isolated microvesicles secreted by colony-stimulating factor 1 (CSF-1)-induced bone marrow-derived macrophages (BMDMs) that were either untreated (UT) or stimulated with interleukin-4 (IL-4). As expected, IL-4 increased the expression of the "alternative macrophage activation" genes *Arg1*, *CD163*, and *Mrc1* in BMDMs (Figure S1A). BMDM-derived microvesicles were highly enriched in particles that had features of exosomes, as shown by physical size analysis by dynamic light scattering (Figure S1B) and protein content by western blotting analysis (Figure S1C). From here on, we refer to macrophage-derived exosomes as "exo-macs."

We profiled the miRNA transcriptome of BMDMs and their exo-macs, either UT (n = 3) or IL-4 treated (IL-4; n = 3), by low-density quantitative PCR (qPCR) arrays. A total of 178 (29%) of the 618 miRNAs present in the arrays were detected in at least two out of three biological replicates of both BMDMs and exo-macs (Table S1). After quantile normalization of the data, 31 miRNAs (5%) were differentially expressed in IL-4-treated versus UT BMDMs (Figure 1A; Table S2A), including miR-138-5p, miR-9-3p (both upregulated; fold-change [FC] = 59 and 16, respectively), miR-146a-5p, and miR-223-3p (both downregulated; FC = 0.10 and 0.27, respectively). We also identified 40 miRNAs (6%) that were relatively increased or decreased in the exo-macs by IL-4 (Figure 1B; Table S2B). These data indicate that IL-4 modulates the expression and/or enrichment of a subset of miRNAs in BMDMs and their exo-macs.

The global miRNA profile greatly differed in BMDMs and exo-macs, regardless of IL-4 stimulation, as shown by the unsupervised hierarchical clustering of the data (Figure 1C). Of the 178 miRNAs detected in all samples, 90 (51%) and 101 (57%) were relatively increased/decreased in the exo-macs compared to UT and IL-4-treated BMDMs, respectively (Figures 1D and 1E; Tables S2C and S2D). Among the miRNAs enriched in the exo-macs were miR-150-5p, miR-146a-5p, miR-320-3p, miR-467b-3p, and miR-467f; of these, miR-150-5p, miR-146a-5p, and miR-320-3p were previously found to be enriched in exosomes derived from distinct cell types (Guduric-Fuchs et al., 2012). Furthermore, 39 miRNAs were relatively increased or decreased in the exo-macs versus BMDMs in an IL-4-dependent manner (e.g., more enriched in exo-macs by IL-4; Figures 1F and 1G; Table S2E).

Although our experimental conditions and analyses cannot measure absolute miRNA abundance in exo-macs and producer BMDMs, they indicate that (1) selected miRNAs are differentially represented in exo-macs and BMDMs (relative to the global miRNA repertoire), and (2) miRNA enrichment in exo-macs is not only miRNA-specific but also dependent on the cell activation state. From here on, we refer to miRNAs contained in exo-macs as "exo-miRNAs."

Artificially Perturbing miRNA or Targeted Transcript Levels Modulates miRNA Sorting to MVBs and Exosomes

Little is known of the molecular regulation of miRNA sorting to exosomes. In order to explore potential mechanisms, we first generated miRNA-deficient BMDMs by transducing bone marrow-derived cells from *Dicer*$^{fl/fl}$ mice with a Cre-expressing LV (Figure S2A). We then analyzed a panel of miRNAs in either *Dicer*$^{fl/fl}$ or *Dicer*$^{-/-}$ BMDMs, and their secreted exo-macs, at day 12 posttransduction, a time point when *Dicer* had been efficiently (albeit nonexhaustively) deleted in the LV-transduced BMDMs (Figure S2B). Intriguingly, miRNA depletion was substantially more prominent in the exo-macs than in the producer, *Dicer*$^{-/-}$ cells, regardless of IL-4 stimulation (Figures 2A and 2B). This was true for each miRNA analyzed and was independent of the expression level of the miRNA in *Dicer*-proficient BMDMs. Thus, upon acute *Dicer* deletion in BMDMs, a moderate miRNA decrease in the cells is associated with a more prominent miRNA depletion in the exo-macs.

To further investigate this phenomenon, we asked whether changes in the abundance of a given miRNA and/or its targets (including artificial and natural targets) could alter miRNA sorting to the exosomes. In order to standardize experimental conditions, we generated a macrophage cell line by immortalizing *Dicer*$^{fl/fl}$ BMDMs with an LV expressing the SV40 large T antigen (Figure S2A). A clonal population of immortalized BMDMs (iBMMs) expressed all analyzed macrophage-specific markers, could be polarized in response to cytokine (IL-4 or LPS plus IFN-γ) stimulation, and was dependent on CSF-1 for survival and growth (Figures S2C–S2F). Furthermore, iBMMs produced bona fide exo-macs, as shown by physical size analysis by dynamic light scattering (Figure S2G), morphology by transmission electron microscopy (Figure S2H), and protein content by western blotting analysis (Figure S2I). Thus, iBMMs represent a suitable surrogate cell line for primary BMDMs.

UT iBMMs express low levels of miR-511-3p, a macrophage-specific miRNA that is induced by IL-4 (Squadrito et al., 2012). We then transduced iBMMs with increasing doses of an LV overexpressing miR-511-3p (Squadrito et al., 2012 and Figure 2C) and analyzed miR-511-3p levels in iBMMs and their exo-macs. Upon increasing overexpression, miR-511-3p levels surged to a greater extent in the exo-macs than in the iBMMs (Figure 2D). Thus, partial miRNA depletion strongly limits (see Figures 2A and 2B) while miRNA overexpression strongly enhances miRNA sorting to exosomes. In a series of parallel experiments, we analyzed the effects of artificially increasing the cellular levels of miR-511-3p target sequences. To this aim, we transduced the iBMMs with increasing doses of an LV expressing eight copies of artificial sequences

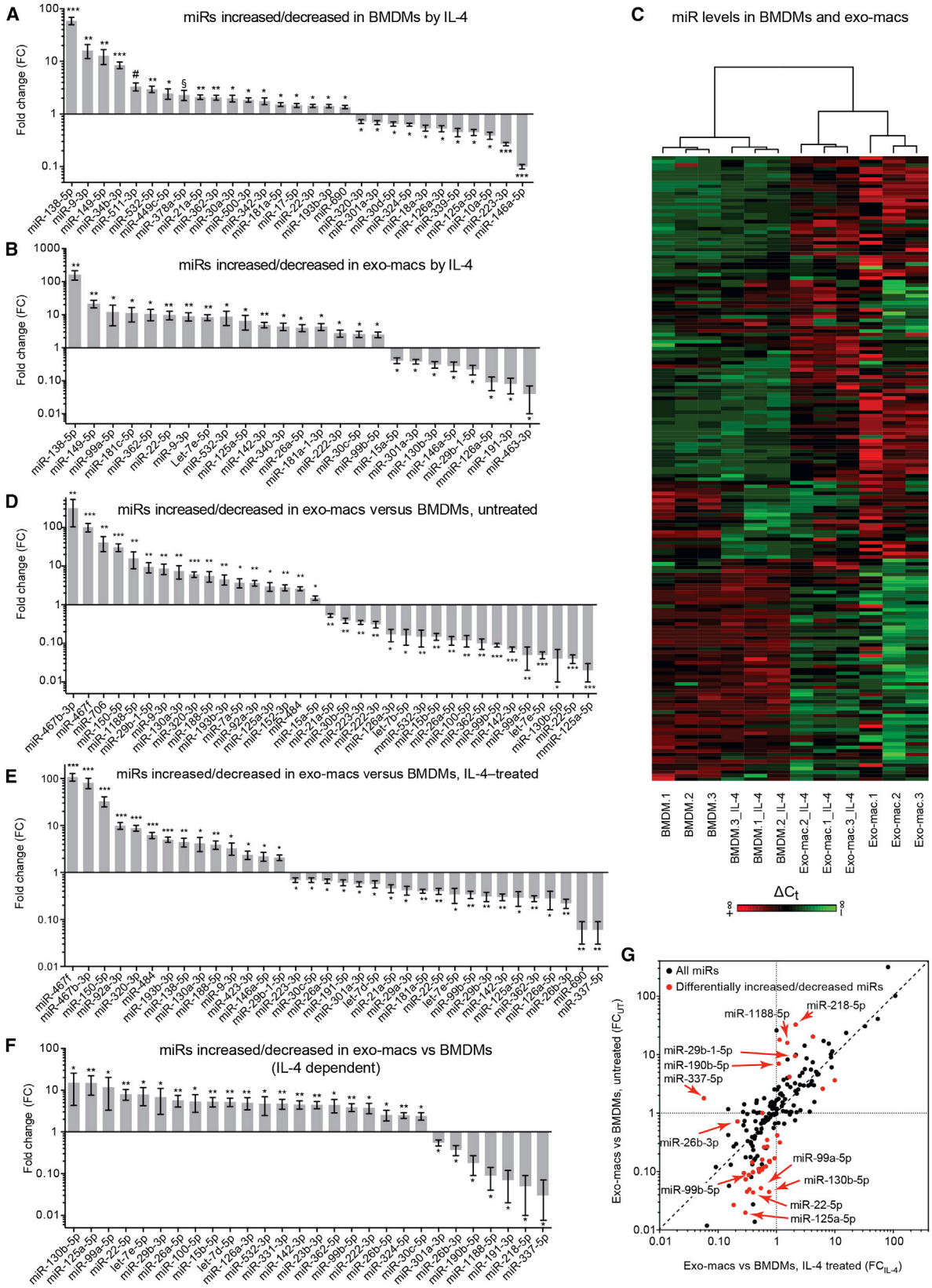

(legend on next page)

with perfect complementarity to miR-511-3p (Figure 2C). Robust overexpression of artificial miRNA target sequences detectably decreased endogenous miR-511-3p levels in the iBMMs (Figure 2E), likely through a "miRNA sponge effect" (Brown and Naldini, 2009; Denzler et al., 2014; Gentner et al., 2009; Mullokandov et al., 2012). However, miR-511-3p levels decreased in the exo-macs to a greater extent than in the iBMMs. Finally, iBMMs engineered to overexpress increasing levels of both miR-511-3p and its target sequences by sequential LV transduction showed that miRNA transfer to exo-macs is controlled by the relative levels of the miRNA and its target sequences in the cell (Figure 2F). Indeed, quantification of miR-511-3p, either after normalization to Let-7a-5p or by absolute copy-number analysis, indicated that maximal overexpression of miR-511-3p target sequences ("artificial targets 2" in Figure 2F) reversed the exosomal enrichment of miR-511-3p that was induced by its overexpression.

While artificial (perfectly complementary) sequences may promote miRNA-dependent cleavage of the target, natural (partially complementary) sequences may cause mRNA destabilization and translation inhibition (Ameres et al., 2007). We then employed natural target sequences for miR-511-3p. We previously validated *Rock2* as a natural target of miR-511-3p (Squadrito et al., 2012). We then transduced iBMMs with increasing doses of an LV expressing a fragment of the *Rock2* 3′ UTR that encompasses target sites for miR-511-3p (*Rock2* 3′UTR LV; Figure 2C). As a control LV, we used *Rock2* 3′ UTR sequences with mutated miR-511-3p binding sites (Squadrito et al., 2012). Whereas natural target sequences did not "sponge" endogenous miR-511-3p detectably in the cells (contrary to artificial sequences; see Figures 2D–2F), they efficiently decreased miR-511-3p levels in the exo-macs (Figure 2G). Taken together, these findings indicate that artificially increasing the abundance of miRNA target sequences limits miRNA levels in the exosomes more markedly than in the producer cells.

MVBs are complex organelles that function as sites of exosome biogenesis (Simons and Raposo, 2009). Based on our finding that artificially increasing the expression of a given miRNA disproportionally increases its levels in the exosomes, we hypothesized that artificially overexpressed miRNAs would also enrich in MVBs. We then performed subcellular fractionation of iBMMs (Gibbings et al., 2009; Stalder et al., 2013) and obtained nine distinct subcellular fractions that were analyzed by western blotting (Figures 3A and S3A). MVBs were enriched in fraction 3 and, to a lesser extent, fractions 2 and 4, as shown by expression of the tetraspanin CD81 (Figure 3A). Fractions 4 to 9 were enriched in endoplasmic reticulum (ER), as shown by expression of calnexin (CNX), whereas fraction 1 and, to a lesser extent, fraction 2 were enriched in P bodies markers, such as AGO2, GW182, and DCP1A, indicative of sites of miRNA activity (Liu et al., 2005). We then transduced iBMMs with a high dose of an LV overexpressing miR-511-3p, or a mutated form (miR-511-3p-mut; Figure S3B; Squadrito et al., 2012), and performed subcellular fractionation. In iBMMs expressing miR-511-3p-mut, endogenous miR-511-3p was detectable, albeit at varying levels, in each fraction (Figure 3B). Overexpressing miR-511-3p increased its levels in all subcellular fractions (data not shown); however, it did so more prominently in the MVB-enriched fraction 3 compared to the other fractions. Conversely, overexpressing artificial (perfectly complementary) or bulge (partially complementary) target sequences for miR-511-3p in the iBMMs (Figure S3B) significantly increased miR-511-3p levels in the P bodies-enriched fraction 1 (Figures 3C and 3D).

Together, these data indicate that artificially increasing the cellular levels of a miRNA or its target sequences favors miRNA enrichment in MVBs (miRNA secretory pathway) and P bodies (miRNA activity pathway), respectively. Thus, fluctuations of natural target levels may have the potential to relocate miRNAs from one cellular compartment to another and tilt the balance between endogenous miRNA activity and secretion through the MVB/exosome pathway.

Cell Activation Modulates miRNA:Target Interactions and Controls miRNA Sorting to Exosomes

Based on the aforementioned findings, we hypothesized that the transcriptional changes that occur in response to cell activation may control miRNA sorting to exosomes by either increasing or decreasing the pool of intracellular miRNA target sequences. To test this hypothesis, we performed RNA-seq of UT (n = 4) and IL-4-treated (n = 4) primary BMDMs. We unequivocally identified ~36,000 transcripts (including protein-coding and noncoding RNAs), of which ~21% were differentially expressed (by edgeR; adjusted p value < 0.05) in the BMDMs upon IL-4 treatment (Figure 4A; Table S3). As expected, IL-4 increased the expression of genes known to be upregulated in alternatively activated macrophages (Martinez et al., 2009), such as *Arg1*, *Retnla*, *Chi3l3* (*Ym1*), *Ccl22*, and *Mrc1* (Figure S4A).

We then implemented a computational model to investigate whether IL-4-induced changes in exo-miRNA levels (see Figures 1 and S1) were dependent on quantitative changes in miRNA target levels in the BMDMs. We first selected miRNAs with at least two out of three determinations in the qPCR array data sets of both BMDMs and exo-macs (178 miRNAs; see Figure 1).

Figure 1. miRNA Analysis in BMDMs and Their Exo-Macs

(A and B) Selected miRNAs (indicated as miRs) increased or decreased in BMDMs (A) and exo-macs (B) by IL-4, analyzed by low-density TaqMan arrays. Data show fold-change (FC) in IL-4-treated versus UT BMDMs/exo-macs (FC = $2^{-\Delta Ct}$, with C_t values normalized by quantile method; mean ± SEM, n = 3). Statistical analysis by moderated t-statistics adjusted for false discovery rate (FDR); *p < 0.05; **p < 0.01; ***p < 0.001, §p = 0.0502. # indicates a miRNA not present in the array and measured separately (FC = $2^{-\Delta\Delta Ct}$, with C_t values normalized to U6; mean ± SEM, n = 3; p = 0.0134; statistical analysis by unpaired Student's t test).

(C) Mean-centered heatmap showing unsupervised hierarchical clustering of miRNA levels in UT (BMDM.1-3) and IL-4-treated (BMDM.1-3_IL-4) BMDMs and their exo-macs (exo-mac.1-3 and exo-mac.1-3_IL-4).

(D and E) Selected miRNAs increased or decreased in exo-macs versus BMDMs, either UT (D) or IL-4 treated (E). Analysis as in (A) and (B).

(F and G) Differential miRNA increase/decrease in exo-macs versus BMDMs by IL-4. (F) Selected miRNAs increased or decreased in exo-macs versus BMDMs by IL-4. Data are shown as FC between FC_{IL-4} and FC_{UT} (mean ± SEM, n = 3). Statistical analysis as in (A) and (B). (G) FC of miRNA levels in exo-macs versus UT (FC_{UT}, y axis) or IL-4-treated (FC_{IL-4}, x axis) BMDMs. miRNAs significantly increased/decreased are shown in red (adjusted p < 0.05; statistical analysis as in A and B).

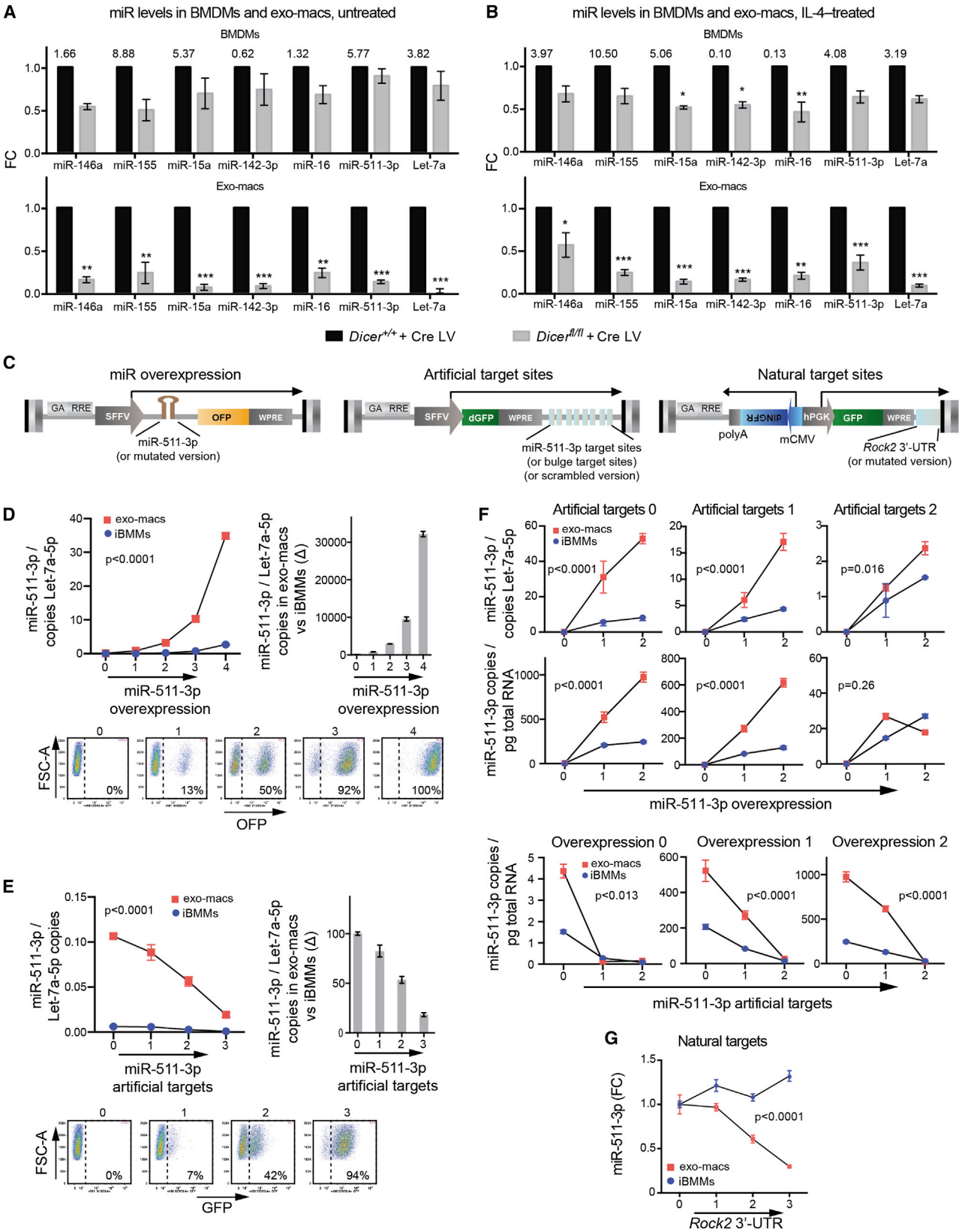

(legend on next page)

We then used the UCSC Genome Browser database (http://genome.ucsc.edu) to select transcripts that contain a 3′ UTR sequence. We identified miRNA target sites (seed:RNA interactions) in each transcript's 3′ UTR and rationally assigned a weight to each of the three main typologies of the seed:RNA interaction (8-mer > 7-mer > 6-mer) to obtain a "weighted interaction score" for each transcript (WIS_t; Supplemental Experimental Procedures). Although 5′ UTRs and open reading frames (ORFs) of mammalian genes contain predicted miRNA target sites, their contribution to miRNA-mediated gene repression is deemed marginal (Bartel, 2009; Grimson et al., 2007); therefore, only 3′ UTR sequences were analyzed. We then used fragments per kilobase per million of reads (FPKM) data to determine, for each miRNA, the weighted interaction score at the transcriptome-wide level (referred to as WIS) in either UT or IL-4-treated BMDMs. Lastly, we calculated the ratio between WIS values in IL-4-treated and UT BMDMs (WIS-ratio). Based on this model, miRNAs whose predicted targets are decreased in BMDMs by IL-4 have a WIS-ratio < 1, or ln(WIS-ratio) < 0, whereas miRNAs whose predicted targets are increased in BMDMs by IL-4 have a WIS-ratio > 1, or ln(WIS-ratio) > 0.

Interestingly, we found a weak but statistically significant anticorrelation ($p < 0.008$) between the WIS-ratio values of miRNAs and their enrichment in the exo-macs (Figures 4B and 4C). The observed anticorrelation was verified also when we employed Δ-WIS values ($p < 0.01$), which measure the absolute increase or decrease (Δ) of the WIS of each miRNA in the transcriptome of IL-4-treated versus UT BMDMs (Figure S4B). Thus, miRNAs whose predicted targets are globally decreased in BMDMs by IL-4 appear to be preferentially enriched in exosomes, and vice versa. It should be noted that we did not observe a statistically significant correlation between WIS-ratio values and differential miRNA expression in IL-4-treated versus UT BMDMs (Figure S4C), suggesting that cell-activation-dependent changes of miRNA target abundance do not globally impact on the cellular miRNA levels.

We then studied the contribution of individual transcripts to the WIS of each of the 178 selected miRNAs. We first ranked the cellular transcripts based on the magnitude of their contribution to the WIS in IL-4-treated versus UT BMDMs (i.e., by using Δ-WIS_t values). We then monitored in silico, for each miRNA the behavior of the WIS in response to the contribution of individual transcripts. We found that, on average, the transcript with highest Δ-WIS_t could contribute to increase or decrease the WIS by ~5% (0.6%–32%; Figure 4D). For example, the matrix metalloproteinase-12 (*Mmp12*) transcript, which is targeted by miR-218-5p and upregulated ~26-fold in IL-4-treated BMDMs (Table S3), increased the WIS of miR-218-5p by ~8% (Figure 4E). Prosaposin (*Psap*; upregulated ~2-fold by IL-4; Table S3) further increased the WIS of miR-218 by ~6%, whereas lysozyme-2 (*Lyz2*; downregulated ~2-fold by IL-4; Table S3; Figure S4D) decreased it by ~4.5%. Of note, the *Mmp12*, *Psap*, and *Lyz2* transcripts are all highly expressed in BMDMs (Figure 4F). When all cellular transcripts were computed, IL-4 increased the WIS of miR-218-5p by ~13.6%. Consistent with the in silico prediction, miR-218-5p levels were relatively lower in the exo-macs derived from IL-4-treated BMDMs than UT BMDMs (see Figure 1E and Table S2E). Among the miRNAs whose WIS decreased after IL-4 was miR-99b-5p (Figure 4E), a miRNA upregulated in the exo-macs in an IL-4-dependent fashion (see Figure 1F). Of note, IL-4 stimulation of BMDMs more frequently increased than decreased the WIS of the investigated miRNAs (Figure 4D).

To validate the aforementioned in silico data, we analyzed the effects of biological *Lyz2* gene knockout on miR-218-5p sorting to exo-macs. To this aim, we used BMDMs obtained from homozygous *Lyz2*.Cre mice (Clausen et al., 1999), which lack both functional copies of *Lyz2* (Figure 4G). As predicted by our model, miR-218-5p, but not miR-16-5p, which does not have binding sites in the 3′ UTR of the *Lyz2* transcript, was enriched in the exo-macs of *Lyz2*.Cre BMDMs compared to wild-type BMDMs (Figures 4H and S4D). Of note, miR-218-5p levels were similar in wild-type and *Lyz2* null BMDMs, suggesting that the *Lyz2* transcript, while containing ~13% of all miR-218-5p binding sites in the coding and noncoding transcriptome, would not modulate the cellular levels of miR-218-5p through a sponge effect.

miRNAs belonging to the same family share the same seed sequence, which controls target recognition (Lai, 2002). Based on our model, miRNA family members should display a similar sorting pattern. To study the behavior of miRNAs that either share or not the same seed sequence, we performed an in silico analysis. We calculated the difference between pairs of fold-change values (Δ-FC) measuring miRNA increase/decrease in exo-macs versus BMDMs by IL-4 (see Figure 1F and Table S2E) for all possible miRNA pairs. We found that miRNA pairs sharing the same seed sequence displayed significantly smaller Δ-FC values than randomly selected miRNA pairs (Figure 4I). Of note, miRNA pairs sharing 3-mer or 4-mer

Figure 2. Changes of miRNA Levels or Their Target Sequences Control miRNA Sorting to Exo-Macs

(A and B) TaqMan analysis of selected miRNAs (indicated as miRs) in $Dicer^{+/+}$ and $Dicer^{fl/fl}$ BMDMs transduced with a Cre-expressing LV, and their exo-macs, either UT (A) or IL-4 treated (B). Data show FC ($FC = 2^{-\Delta\Delta Ct}$, with C_t values normalized to U6; mean ± SEM, n = 2–3) versus LV-transduced $Dicer^{+/+}$ BMDMs (black bars, upper panels) or their exo-macs (black bars, bottom panels). In the top panels, miRNA ΔC_t values (versus U6) are indicated for BMDMs. Statistical analysis by two-way ANOVA, with Sidak's multiple comparisons test.

(C) Schematics of proviral LVs.

(D and E) Top graphs show miR-511-3p levels (D, normalized to Let-7a-5p; E, difference between normalized levels in exo-macs versus cells) in iBMMs and exo-macs. iBMMs were transduced with increasing doses (D, 1–4; E, 1–3) of LVs either overexpressing miR-511-3p (D) or its artificial target sequences (E); dose 0 indicates untransduced iBMMs. FACS dot plots on the bottom show iBMMs transduced as indicated. Statistical analysis by analysis of covariance (ANCOVA).

(F) miR-511-3p levels in iBMMs and exo-macs. iBMMs were cotransduced with increasing doses of LVs overexpressing miR-511-3p or its artificial target sequences, as indicated. miR-511-3p levels were either normalized to Let-7a-5p or shown as absolute miRNA copies per pg of total RNA. Statistical analysis by ANCOVA.

(G) miR-511-3p levels normalized to Let-7a-5p in iBMMs and exo-macs. iBMMs were transduced with increasing doses (1–3) of an LV expressing a fragment of the *Rock2* 3′ UTR. Data show FC versus exo-macs or iBMMs transduced with a mutated *Rock2* 3′ UTR (mean ± SEM, n = 3). Statistical analysis by ANCOVA.

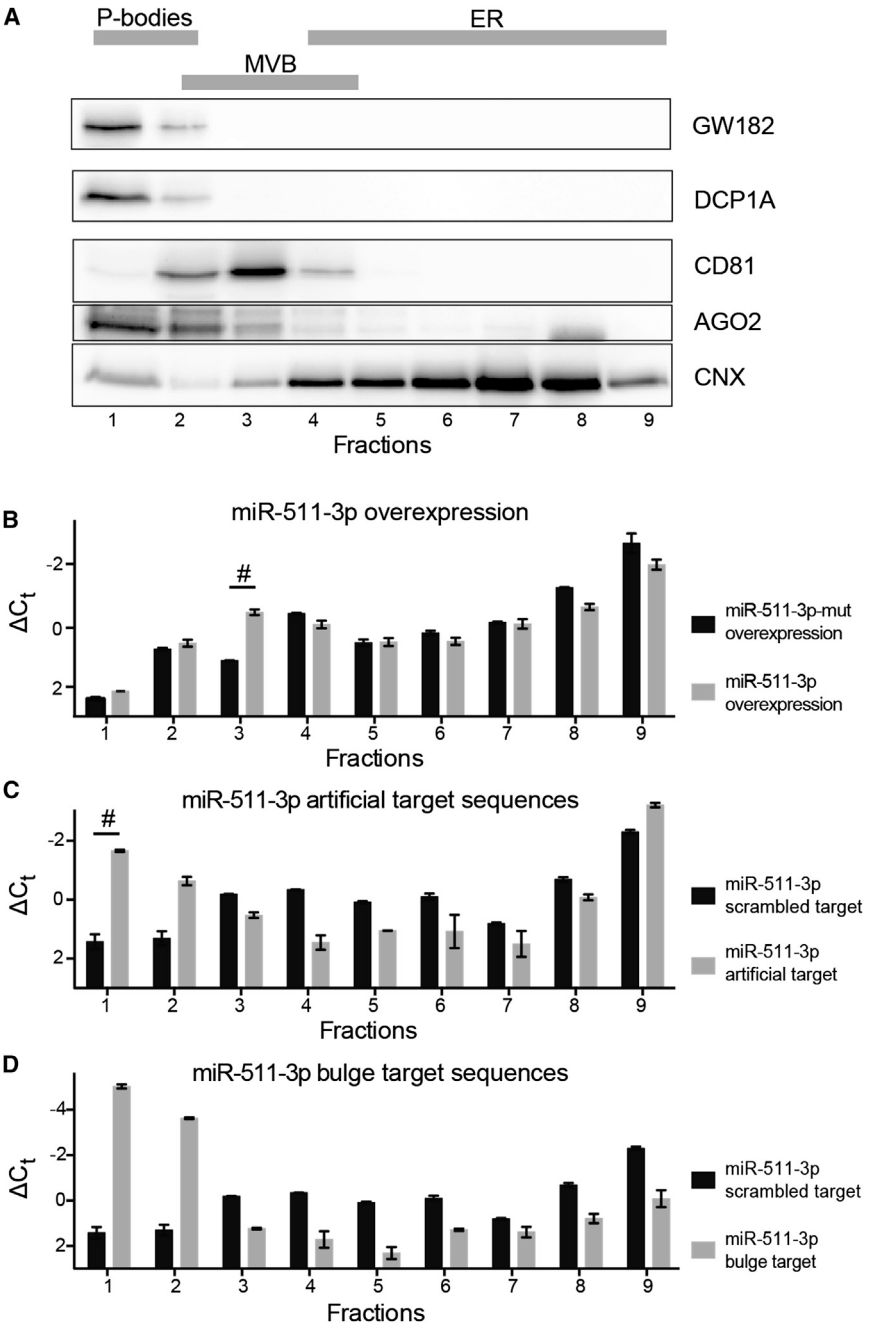

Figure 3. Relocation of miRNAs to Distinct Subcellular Compartments

(A) Western blotting analysis of subcellular fractions obtained from iBMMs. Three of six independent experiments are shown.

(B–D) miR-511-3p levels in subcellular fractions obtained from iBMMs transduced with LVs overexpressing miR-511-3p (B, versus miR-511-3p-mut), its artificial (perfectly complementary) target sequences (C, versus scrambled target), or its bulge (nonperfectly complementary) target sequences (D, versus scrambled target). For each fraction, miRNA levels are shown as ΔC_t values (difference between the C_t in the fraction of interest and the mean C_t calculated on all fractions). One representative experiment of three performed is shown for (B) and (C); statistical analysis of the data was performed on the three biological replicates (B and C) by two-way ANOVA, with Sidak's multiple comparison test (#$p < 0.01$).

sequences located outside the seed sequence behaved similarly to random miRNA pairs.

Taken together, our results suggest that the cellular levels of natural miRNA targets, which dynamically change in response to cell activation, may modulate miRNA enrichment in exosomes without detectably affecting the cellular miRNA levels.

Macrophage-Derived Exosomes Transfer miRNA Activity to Acceptor Endothelial Cells

Macrophages modulate EC biology and stimulate angiogenesis by secreting growth factors and matrix-remodeling enzymes (Baer et al., 2013). Furthermore, miRNA transfer via exosomes may mediate macrophage-to-EC communication and, therefore, potentially influence macrophage-regulated angiogenesis. In order to visualize and measure exo-mac transfer to ECs, we generated fluorescently labeled exo-macs by transducing iBMMs with an LV expressing a CD9 cDNA fused with either mCherry (SFFV.CD9.mCherry) or enhanced GFP (SFFV.CD9.eGFP) (Figure S5A). Fluorescence spectroscopy showed readily measurable, proteinase-resistant mCherry fluorescence in the exo-macs (Figures S5B–S5D). In order to study exo-mac transfer, we established immortalized, endothelial-like cells (iELCs) from the heart of *Dicer*$^{fl/fl}$ mice and treated them with increasing doses of mCherry^{+} exo-macs. Flow cytometry of iELCs showed dose-dependent mCherry fluorescence (Figure S5E). iELCs rapidly internalized exo-macs (Figure S5F), which became evident in the cell cytoplasm as punctate mCherry staining (Figure S5G). A similar intracellular pattern of mCherry was observed when iELCs were cocultured with CD9.mCherry^{+} iBMMs (Figure S5H). LAMP1 staining of iELCs, or their transduction with a LAMP1-eGFP fusion protein (Lysotracker), indicated that a significant proportion of the mCherry signal colocalized with late endosomes/lysosomes (Figures S5I and S5J), as previously shown in other studies (Morelli et al., 2004). Whereas these data show a rapid and dose-dependent exo-mac uptake by ECs, they also indicate that a sizable proportion of the uptaken exo-macs enter the endocytic pathway and are possibly degraded in lysosomes.

To measure exo-miRNA transfer from macrophages to ECs, we cocultured an EC line, bEND.3, with iBMMs in transwell

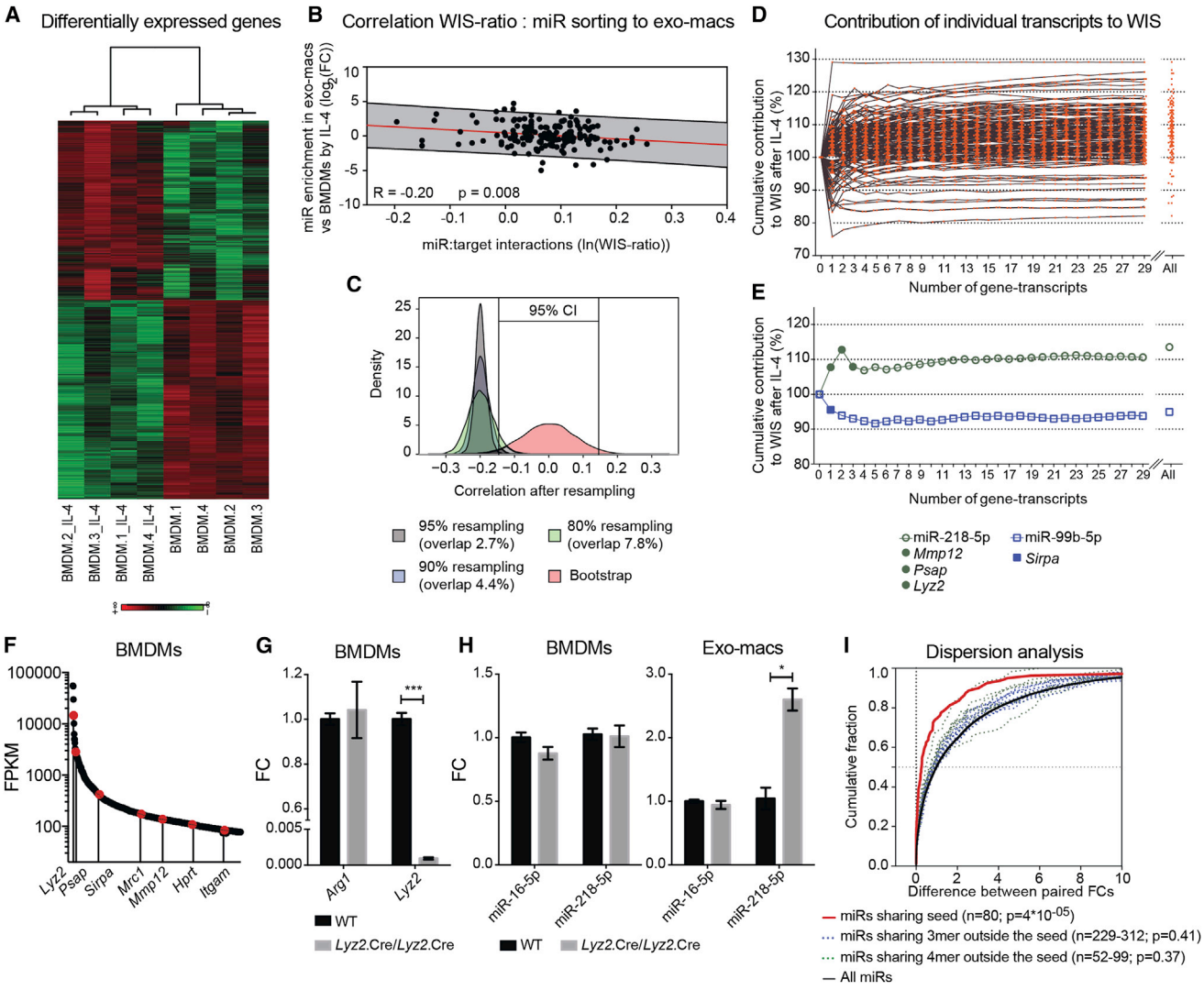

Figure 4. Gene Transcript Levels Modulate miRNA Sorting to Exo-macs

(A) Mean-centered, hierarchical clustering of genes differentially expressed in UT (BMDM.1-4) and IL-4-treated (BMDM.1-4_IL-4) BMDMs.

(B) Correlation between the WIS-ratio [shown as ln(WIS-ratio)] and miRNA (indicated as miR) enrichment in exo-macs [versus BMDMs; shown as $\log_2$(FC) of miRNA levels] after IL-4 treatment of BMDMs. The gray area identifies 95% of the events (95% prediction band).

(C) Bootstrap analysis of the data in (B) performed by randomly assigning $\log_2$(FC) to ln(WIS-ratio) values for 10^4 times (red curve, showing the distribution of R values). The black, blue, and green curves show the distribution of R values obtained by removing 20%, 10%, and 5%, respectively, of the ln(WIS-ratio) and $\log_2$(FC) values from the analysis in (B). The overlap between the random distribution and the resample distribution is indicated. The vertical lines identify confidence interval (CI = 95%).

(D and E) Cumulative contribution of individual transcripts to the WIS (D, all detected miRNAs; E, selected miRNAs) in IL-4-treated versus UT BMDMs.

(F) Transcripts with FPKM values >80 as detected in BMDMs by RNA-seq. Selected transcripts are indicated.

(G) TaqMan analysis of the indicated genes (normalized to *B2m*) in IL-4–treated BMDMs. Data show mean values (±SEM, n = 3). Statistical analysis by unpaired Student's t test.

(H) TaqMan analysis of miR-16-5p and miR-218-5p (normalized to U6) in IL-4-treated BMDMs (left) and their exo-macs (right). Data show mean values (±SEM, n = 3). Statistical analysis by unpaired Student's t test.

(I) Cumulative distribution of the difference between FC values (Δ-FC; see Figure 1F and Table S2E) of individual miRNA pairs sharing the same seed sequence (nucleotides in position 2–8; red line), all 3-mer/4-mer sequences outside the seed (blue/green lines), or randomly selected miRNA pairs (black line). Statistical analysis by Kolmogorov-Smirnov test.

assays. We then used low-density qPCR arrays to interrogate the miRNA transcriptomes of ECs that were cultured either alone or with iBMMs. Whereas the global miRNA transcriptome of ECs was not significantly modulated by their coculture with iBMMs (data not shown), selected miRNAs were significantly increased (Figure 5A). Of these, a sizable proportion was miRNAs that displayed a relatively high enrichment in the exo-macs compared to ECs. Indeed, miRNAs that were >10-fold higher in exo-macs

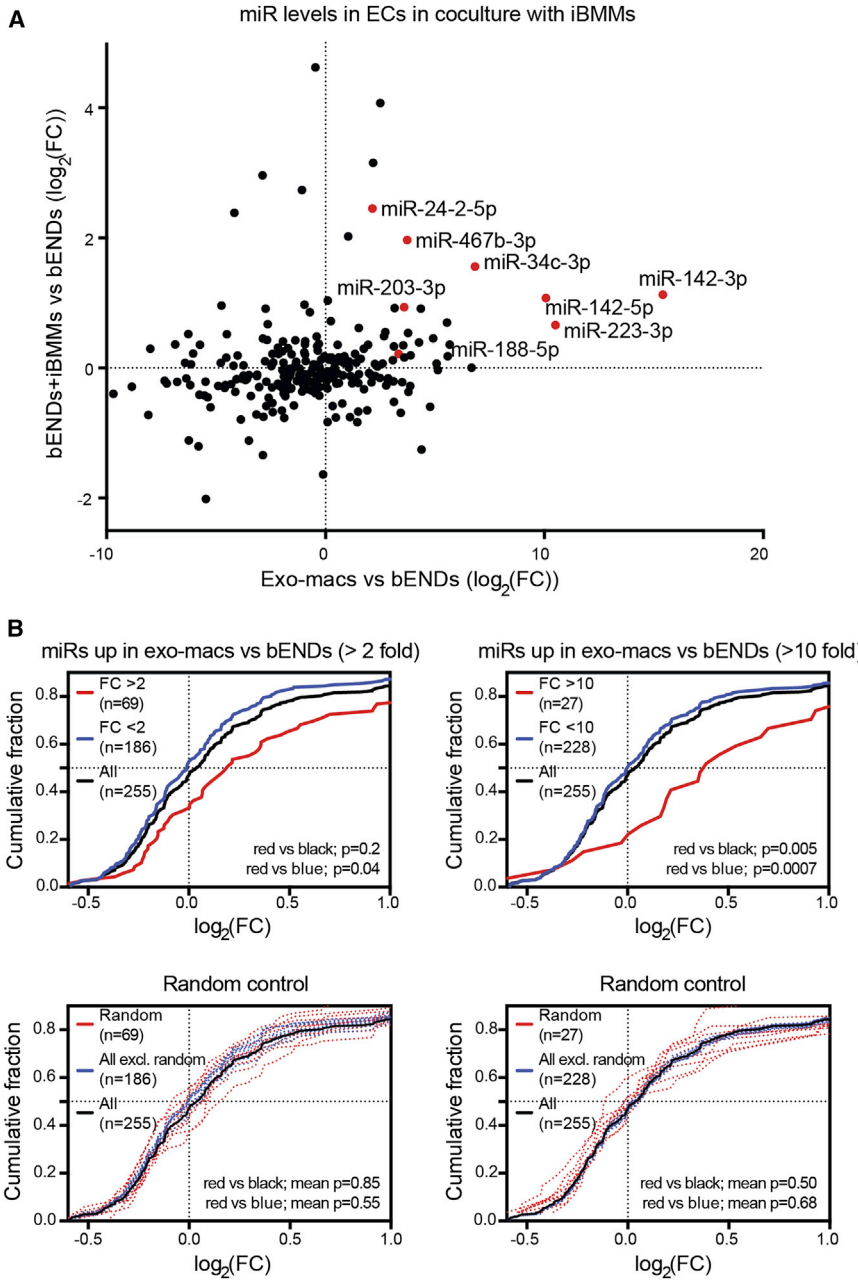

Figure 5. Global miRNA Transfer from iBMMs to ECs upon Coculture

(A) Correlation between miRNA (indicated as miR) levels in exo-macs from IL-4-treated iBMMs [$\log_2$(FC) versus bENDs; x axis] and miRNA levels in bENDs in coculture with IL-4–treated iBMMs [$\log_2$(FC) versus bENDs; y axis]. Data show independent experiments combined (n = 3 for exo-macs; n = 2 for bENDs). miRNAs of interest are indicated by red dots.

(B) Cumulative distribution of the FCs of miRNA levels in bENDs in coculture with IL-4-treated iBMMs versus bENDs. The black lines show FCs of all miRs; the red lines show FCs of miRNAs that are upregulated in exo-macs from IL-4-treated iBMMs versus bENDs by >2-fold (top left) or >10-fold (top right); the blue lines show FCs of miRNAs that are upregulated in exo-macs from IL-4-treated iBMMs versus bENDs by <2-fold (top left) or <10-fold (top right). Bottom panels show cumulative FCs using randomly selected miRNAs (using the same number of miRNAs analyzed in the top panels). Statistical analysis by two-sided Kolmogorov-Smirnov test.

than ECs were globally and significantly increased in the ECs upon coculture with iBMMs (Figure 5B). For example, miR-142-3p and miR-223-3p, which are highly expressed in iBMMs and their exo-macs but virtually undetectable in ECs, were significantly increased in ECs cocultured with iBMMs (Figure 5A). Together, these data suggest the occurrence of miRNA transfer from macrophages to ECs in vitro.

We then asked whether exo-miRNAs can repress target genes in ECs. To this aim, we constructed a panel of 32 miRNA reporter LVs, each incorporating two miRNA target (miRT) sequences with perfect complementarity to a given miRNA into the 3′ UTR of a destabilized GFP (dGFP) transgene, which is expressed from a ubiquitously active bidirectional promoter that also controls the expression of the reporter gene, ΔLNGFR (Figure S6A). We also generated a control LV expressing a dGFP sequence not containing miRT sequences in its 3′ UTR (termed no-miRT). Following LV cell transduction, the miRNA machinery will degrade the dGFP transcript containing miRT sequences only in the cells that express the cognate miRNA, in a manner that is dependent on miRNA abundance and/or activity. On the other hand, expression of ΔLNGFR is independent of miRNA activity and is used as an internal normalizer to calculate GFP fold repression as a direct readout of miRNA activity, as described previously (Brown et al., 2007; Mullokandov et al., 2012; Squadrito et al., 2012).

We first measured endogenous miRNA activity in IL-4-treated iBMMs and ECs (bEND.3). We found that several miRNAs were highly active in both cell types, such as miR-21a-5p, miR-24-3p, Let-7e-5p, and Let-7a-5p (Figure S6B). Other miRNAs showed specific and/or high activity in either cell type, such as miR-142-3p, miR-511-3p (specifically active in iBMMs), miR-92a-3p, and miR-125a-5p (highly and specifically active in ECs). In order to measure functional exo-miRNA transfer, iELCs expressing miRNA reporter LVs were incubated with exo-macs from IL-4-treated iBMMs. The exo-macs were readily uptaken by and transferred miRNA activity to iELCs (+10%–20% miRNA activity compared to cells not exposed to exo-macs; Figures S6C–S6E). To rule out de novo endogenous miRNA activity, we transduced

Dicer$^{fl/fl}$ iELCs with a hPGK.Cre-Puro LV (Figure S2A) and selected a *Dicer*$^{-/-}$ iELC clone for subsequent experiments (Figure S6F). As expected, endogenous miRNA activity was globally disrupted in *Dicer*$^{-/-}$ iELCs (Figure 6A), although Let-7 family members displayed residual activity, possibly due to DICER-independent miRNA processing (Cifuentes et al., 2010). Of note, we found substantially lower miRNA activity in *Dicer*$^{-/-}$ than *Dicer*$^{fl/fl}$ iELCs following their incubation with exo-macs (Figure S6G). This observation suggests that low-level exo-miRNA activity may be masked by endogenous miRNA activity induced by cell treatment with exosomes.

We then asked whether continuous exposure of ECs to macrophages would increase transfer of exo-miRNA activity. Coculturing iBMMs with *Dicer*$^{-/-}$ iELCs led to substantial transfer of miRNA activity from the macrophages to ECs (+10%–40% miRNA activity compared to cells not cocultured with iBMMs; Figure 6B). We then compared miRNA activity in different ECs (bEND.3, *Dicer*$^{fl/fl}$ and *Dicer*$^{-/-}$ iELCs) either treated with exo-macs or cocultured with iBMMs. We consistently found increased activity of selected miRNAs, including Let-7e-5p, miR-142-3p, miR-188-5p, miR-146a-5p, and miR-150-5p, in the ECs (Figures 6B–6E; Figures S6E and S6G). Of note, the aforementioned miRNAs are either highly expressed in macrophages (e.g., miR-142-3p and miR-146a-5p) or enriched in the exo-macs (e.g., miR-146a-5p, miR-188-5p, miR-150-5p, and miR-467f; see Figure 1).

We then selected two exo-miRNAs, miR-188-5p and miR-142-3p, for further validation experiments. Importantly, transfer of miRNA activity to *Dicer*$^{-/-}$ iELCs was greatly decreased when exo-macs were isolated from miRNA-depleted, *Dicer*$^{-/-}$ iBMMs (Figure 6F), demonstrating genuine transfer of exo-miRNA activity from macrophages to ECs in vitro. Finally, in order to study functional exo-miRNA transfer in vivo, we inoculated Matrigel plugs containing *Dicer*$^{-/-}$ iELCs transduced with a miR-142-3p reporter LV (or a no-miRT LV), with or without CD9.mCherry^{+} iBMMs, subcutaneously in athymic (*nu/nu*$^{-/-}$) mice. Eight days later, we analyzed the Matrigel plugs by flow cytometry. Both the percentage and mCherry mean fluorescence intensity (MFI) of the endogenous CD31^{+} ECs were significantly higher in implants containing CD9.mCherry^{+} iBMMs (Figure 6G), therefore showing exo-mac fusion with ECs in vivo. Moreover, both the mCherry MFI and miR-142-3p activity were increased in the *Dicer*$^{-/-}$ iELCs from implants containing CD9.mCherry^{+} iBMMs (Figures 6H and 6I), indicating bona fide transfer of exo-miRNA activity from macrophages to ECs in vivo.

DISCUSSION

The results of this study suggest that miRNA availability for exosomal secretion is controlled, at least in part, by the cellular levels of their targeted transcripts. By employing both transcriptomic analyses and LV-reporter based assays, we found that either physiological (cell-activation-dependent) or artificial overexpression of miRNA target sequences promotes a relative miRNA enrichment in P-bodies and depletion from MVBs and exosomes. Conversely, artificial overexpression of a miRNA enriches it in MVBs and exosomes. These results were corroborated by implementing a computational model to identify miRNA:target interactions at the genome-wide level. IL-4-stimulated macrophages were selected as a cellular system based on our finding, as well as extensive previous work (Martinez et al., 2009), that IL-4 activates macrophages by skewing the expression of a large proportion of genes. By comparing IL-4-treated and UT macrophages, the model revealed a statistically significant, negative correlation between miRNA:target interactions in the cells and miRNA enrichment in exosomes. These findings may imply that exosomal miRNA secretion is a mechanism whereby cells rapidly dispose miRNAs in excess of their targets to adjust miRNA:mRNA homeostasis.

miRNA:mRNA interactions were computed by considering canonical seed:target matches predicted to occur among all miRNAs and gene transcripts that were detected in our transcriptomic data sets. Although short-sequence interactions (6-mers) account for the vast majority of the predicted seed:target matches (~70%), they contain many false positives and have low specificity and precision (Ellwanger et al., 2011). miRNA:target prediction algorithms like TargetScan therefore favor seed:target matches with longer over shorter sequence (Ellwanger et al., 2011; Grimson et al., 2007). To take these considerations into account, the three main categories of seed:target matches (i.e., 6-mer, 7-mer, and 8-mer) were assigned a weighted score (0.3, 0.7, and 1.0, respectively) to minimize the contribution of false positives (which are more prevalent among 6-mers) and emphasize that of the most robust seed:target matches (8-mers). For the sake of simplicity, our model did not consider other miRNA/target features that may predict miRNA activity, such as the conservation of the seed:target match, the nucleotide composition of the seed:target flanking regions, and free energy-based determinants, among others (Wen et al., 2011). Moreover, we only considered seed:target matches in the 3′ UTR and excluded those in the 5′ UTR and ORF of the transcript. Several studies have indeed shown that miRNA-binding sites in ORFs and 5′ UTRs contribute minimally to miRNA activity (Baek et al., 2008; Grimson et al., 2007); therefore, computing such interactions in our model would have likely increased the proportion of false positives. For the same reason, we did not consider noncanonical miRNA binding sites, such as bulge seed:target interactions and those containing G:U matches (Helwak et al., 2013). Because we implemented simplified criteria aimed to minimize potential false positives, it is possible that our results neglect the contribution of a fraction of the miRNA:target interactions to exo-miRNA biogenesis and hence underestimate the breadth of the phenomenon. In addition to the contribution of the aforementioned factors, the relative weakness of the anticorrelation suggests the very likely scenario that additional mechanisms regulate miRNA sorting to exosomes, such as miRNA family and sequence-specific or biogenesis-dependent mechanisms (Kosaka et al., 2010; Villarroya-Beltri et al., 2013).

Several reports have shown that miRNA activity is higher in cytoplasmic granules known as GW or P bodies, where proteins that have a key role in translation repression, such as GW182 and AGO2, have been shown to colocalize with untranslated mRNAs (Jakymiw et al., 2005; Liu et al., 2005; Pillai, 2005). Of note, GW/P bodies localize in close proximity to MVBs (Gibbings et al., 2009), which are involved in exosome biogenesis. It is therefore

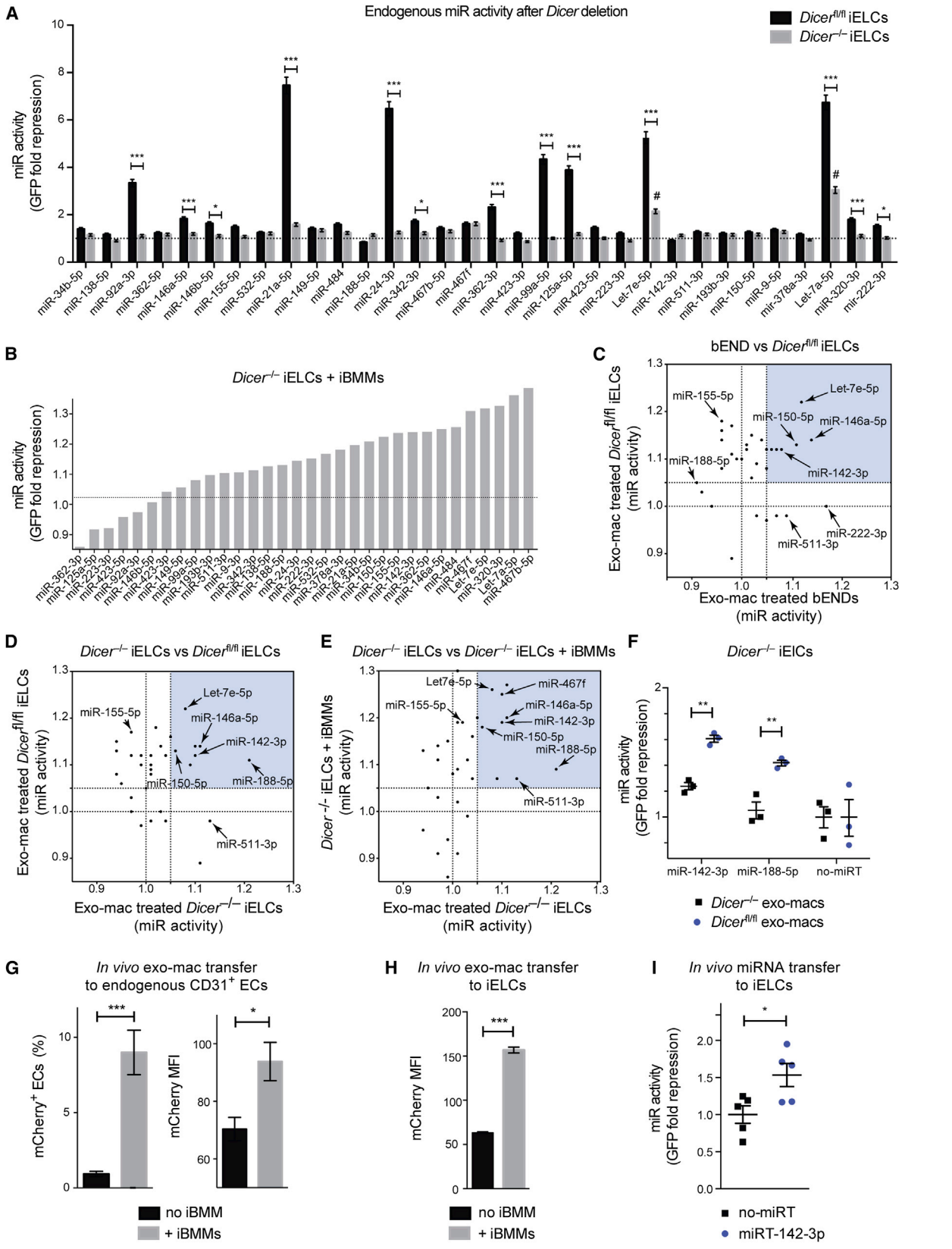

(legend on next page)

tempting to speculate that miRNAs may passively traffic from GW/P bodies to MVBs in response to oscillations of target mRNA levels associated with such organelles. Recent studies have also shown that miRNA activity may colocalize, at least in part, with other subcellular compartments, such as the rough ER (Stalder et al., 2013).

It has been proposed that the natural targets of a given miRNA may act as ''competing endogenous RNAs'' (ceRNAs) that regulate miRNA bioavailability by competing with each other for miRNA binding (Cesana et al., 2011; Poliseno et al., 2010; Tay et al., 2011, 2014). For example, it was found that the *PTEN* pseudogene, *PTENP1*, whose 3′ UTR is highly homologous to that of *PTEN* and contains many miRNA target sites, upregulates PTEN expression by competing with *PTEN* for the binding to miRNAs (Poliseno et al., 2010). In another study, a human circular RNA antisense to *CDR1* (termed *CDR1as*) operated as a miRNA antagonist by sequestering miR-7 through 63 conserved sites present in its sequence (Memczak et al., 2013). Our data (Figures 2E and 2F) are in line with previous reports that exceedingly high copies of a miRNA target are required in a cell to disrupt miRNA activity through a ''sponge effect'' (Baccarini et al., 2011; Brown and Naldini, 2009; Denzler et al., 2014; Gentner et al., 2009). For example, we found that the genetic knockout of *Lyz2*, which contributes to almost 3% of all the total transcripts and at least 13% of the target sites for miR-218-5p in BMDMs, did not affect the cellular levels of miR-218-5p but significantly increased its loading into exosomes. Thus, changes in endogenous target levels that are insufficient to detectably alter miRNA abundance (and possibly activity) in the cell may have the potential to modulate miRNA sorting to exosomes through a ''miRNA relocation effect'' likely regulated by the relative amounts of bound versus unbound miRNA and unknown mechanisms of subcellular miRNA compartmentalization (Ameres et al., 2010; Baccarini et al., 2011; Mullokandov et al., 2012).

While our findings suggest that miRNA sorting to exosomes may be a passive mechanism to dispose miRNAs in excess of their cellular targets, increasing data indicate that exosomes can be actively internalized by other cells, resulting in miRNA transfer among cells of both homo- and heterotypic nature (Hergenreider et al., 2012; Mittelbrunn et al., 2011; Ramachandran and Palanisamy, 2012; Simons and Raposo, 2009; Skog et al., 2008; Valadi et al., 2007). Furthermore, extracellular miRNAs may represent biomarkers of disease and response to therapy. For example, cancer cells display altered transcriptomic profiles, which in turn may differentially modulate miRNA sorting to exosomes. Certain miRNA signatures identified in serum exosomes indeed have both diagnostic and prognostic power for some cancer types (Manterola et al., 2014; Pigati et al., 2010; Skog et al., 2008).

Although miRNAs can traffic among cells via exosomes and other microvesicles, the significance of exogenously derived miRNAs for the global miRNA activity of a cell remains unclear. To rigorously quantitate the effects of exosome-mediated miRNA transfer in a model of macrophage-to-EC communication, we generated *Dicer*-deficient ECs and exposed them to exosomes from either *Dicer*-proficient or *Dicer*-deficient macrophages. Although we detected bona fide transfer of miRNA activity via exosomes, the contribution of exogenously derived miRNAs to target gene repression was overall modest. While our findings indicate that most of the exo-macs uptaken by ECs end up in lysosomes, suggesting degradation of their miRNA content, they do not exclude the possibility that certain tissue microenvironments, such as tumors (Baer et al., 2013) or atherosclerotic plaques (Hergenreider et al., 2012), may facilitate miRNA transfer among cells by producing profuse amounts of miRNA-enriched exosomes. Indeed, macrophages abundantly enwrap immature blood vessels in tumors, a process that may enhance exo-mac fusion with ECs and, consequently, miRNA transfer to ECs engaged in angiogenesis (Baer et al., 2013; Squadrito et al., 2013).

In summary, our data indicate that dynamic transcriptomic changes that occur in response to cell activation may modulate miRNA sorting to exosomes, at least in part, by differentially engaging them at sites of miRNA activity (P bodies) and exosome biogenesis (MVBs). Such mechanism of miRNA compartmentalization regulated by miRNA targets may have implications for exosome-mediated miRNA transfer and intercellular communication.

EXPERIMENTAL PROCEDURES

Additional or more detailed experimental procedures are available in the Supplemental Experimental Procedures.

Lentiviral Vector Construction

Detailed information (sequences, primers, and cloning strategies) is available in the Supplemental Experimental Procedures.

miRNA Reporter LVs

Thirty-two different miRNA reporter LVs were generated by introducing two tandem sequences with perfect complementarity to specific miRNAs (miRT

Figure 6. In Vivo Transfer of Exosomes and miRNA Activity from Macrophages to ECs

(A) Endogenous miRNA (indicated as miR) activity in *Dicer*$^{fl/fl}$ (n = 2) and *Dicer*$^{-/-}$ iELCs (n = 4) measured by miRNA reporter LVs, shown as GFP fold-repression normalized to iELCs transduced with a no-miRT control LV. Statistical analysis by two-way ANOVA, with Sidak's multiple comparison test. # indicates miRNAs that display activity after *Dicer* deletion.

(B) miRNA activity in *Dicer*$^{-/-}$ iELCs in coculture with iBMMs (versus *Dicer*$^{-/-}$ iELCs; n = 2), measured by miRNA reporter LVs (normalized to a no-miRT LV).

(C–E) miRNA activity in either iELCs or bENDs treated as indicated (versus UT), measured by miRNA reporter LVs (normalized to a no-miRT LV). miRNAs in the blue quadrant are recurrently increased in the ECs both by exo-mac treatment and coculture with iBMMs.

(F) miR-142-3p and miR-188-5p activity (normalized to a no-miRT LV) in *Dicer*$^{-/-}$ iELCs treated with exo-macs from either *Dicer*$^{fl/fl}$ or *Dicer*$^{-/-}$ iBMMs (three biological replicates and two independent experiments, of which one is shown). Statistical analysis by two-way ANOVA, with Sidak's multiple comparison test.

(G–I) Flow cytometry analysis of ECs from Matrigel plugs either containing CD9.mCherry^{+} iBMMs (n = 7) or not (n = 13). (G) Percentage of mCherry^{+} ECs (left) and mCherry MFI of endogenous CD31^{+} ECs (right); percentage values were converted to arcsin values and statistical analysis performed by unpaired t test. (H) mCherry MFI of ΔLNGFR^{+} *Dicer*$^{-/-}$ iELCs; statistical analysis by unpaired Student's t test. (I) miR-142-3p activity (normalized to a no-miRT LV) in ΔLNGFR^{+} *Dicer*$^{-/-}$ iELCs in implants containing CD9.mCherry^{+} iBMMs (n = 5); statistical analysis by unpaired Student's t test.

sequences) downstream to a destabilized GFP (dGFP) transgene expressed from a bidirectional LV also encoding for a ΔLNGFR transgene (Amendola et al., 2005).

LVs for Overexpression of miR-511-3p or Its Target Sequences

LVs to overexpress miR-511-3p, or its mutated form, were described previously (Squadrito et al., 2012). LVs to overexpress artificial or natural target sequences for miR-511-3p are based on a SFFV.dGFP LV, which exploits the strong SFFV promoter to overexpress a dGFP transgene linked to eight tandem sequences with complementarity to a given miRNA (Gentner et al., 2009). Natural target sequences for miR-511-3p were obtained from the *Rock2* 3′ UTR, as described previously (Squadrito et al., 2012).

LV to Express Cre Recombinase or Immortalize BMDMs

The Cre LV was generated by replacing the ΔLNGFR and the GFP DNA sequences of a bidirectional LV (Amendola et al., 2005) with Cre and puromycin resistance (Puro) coding sequences, respectively. The SV40 large T antigen (TAg) coding sequence (a gift from Didier Trono, EPFL) was cloned in an SFFV promoter-containing LV (Squadrito et al., 2012).

Exosome Isolation

In order to isolate exo-macs, BMDMs and iBMMs were cultured in serum-free medium (SFM medium; Life Technologies). In coculture experiments (e.g., iBMMs with ECs), culture medium was supplemented with FBS previously depleted of exosomes by ultracentrifugation at 134,000 × *g* for 6 hr. In order to isolate exo-macs, we employed two different techniques: (1) ExoQuick TC (System Biosciences), for primary BMDMs; and (2) ultracentrifugation, for iBMMs. Exo-macs were used immediately or stored at −80°C. Detailed protocols are available in Supplemental Experimental Procedures.

Low-Density miRNA TaqMan Arrays

The Rodent MicroRNA TaqMan Array (Life Technologies) was used to profile miRNAs in BMDMs; IL-4-treated BMDMs; bEND.3; bEND.3 cocultured with macrophages; exo-macs from UT BMDMs; and exo-macs from IL-4-treated BMDMs. The data were collected and processed using the SDS2.4 software (Life Technologies). miRNAs that had fewer than two out of three determinations per condition were excluded from the analysis. C_t values were normalized using the quantile method. Additional information is available in the Supplemental Experimental Procedures.

RNA-Seq of BMDMs

UT (n = 4) and IL-4-treated (n = 4) BMDMs were lysed in Qiazol and total RNA extracted. Total RNA was then depleted of rRNA using the Ribo-Zero RNA removal kit (Epicenter Biotechnologies). Illumina sequencing libraries were prepared according to the TruSeq RNA v2 Sample Preparation Guide (Revision B) and sequencing performed on a HiSeq 2500 (Illumina) using paired-end cBot v3 clustering and TruSeq SBS reagents. Libraries were sequenced using 2 × 100 bp paired-end reads. The 100 nt paired-end reads were then mapped to mm9 reference genome using Tophat software version 2.0.9, with default options, using mm9 UCSC reference genes GTF. Count data for each exon were generated using htseq-count from the HTseq package (http://www-huber.embl.de/users/anders/HTSeq/; version 0.5.4p3). Fragments per kilobase per million of reads (FPKM) were estimated for transcripts in each of the conditions using the cufflinks software (version 2.1.1). Additional information is available in the Supplemental Experimental Procedures.

Gene/miRNA Expression Analysis by TaqMan Arrays and RNA-Seq

Differentially expressed mature miRNAs (TaqMan arrays) and gene transcripts (RNA-seq) were identified using the limma package in R. For gene transcripts, the raw read counts per gene were first filtered for minimal expression (average of raw counts was more than five across samples), normalized to the relative size of each library using the R package edgeR, and then transformed to log2-cpm (counts per million reads) using the voom function. Empirical Bayes moderated t statistics and corresponding p values were then computed for the comparison (IL-4-treated versus UT BMDMs/exo-macs). p values were adjusted for multiple comparisons using the Benjamini Hochberg procedure. Gene transcripts and miRNAs with an adjusted $p \leq 0.05$ were considered to be differentially expressed. Additional information is available in Supplemental Experimental Procedures.

Statistical Analysis

Statistical analysis of the data is described in the figure legends. Error bars show mean values ± SEM, unless stated otherwise. Statistical significance of the data is indicated as follows: *p < 0.05; **p < 0.01; ***p < 0.001.

ACCESSION NUMBERS

RNA-seq data (eight BMDM samples) have been deposited to the NCBI Gene Expression Omnibus under accession number GSE58283.

SUPPLEMENTAL INFORMATION

Supplemental Information includes Supplemental Experimental Procedure, six figures, and three tables and can be found with this article online at http://dx.doi.org/10.1016/j.celrep.2014.07.035.

AUTHOR CONTRIBUTIONS

M.L.S. designed and performed research, constructed LVs, devised the bioinformatic model for analyzing miRNA:target interactions, analyzed data, and wrote the manuscript. C.B. designed and performed research, analyzed data, and wrote the manuscript. F.B. and M.I. analyzed RNA-seq and miRNA TaqMan array raw data and developed (along with M.L.S.) the bioinformatic model for analyzing miRNA:target interactions. C.M. performed research and produced LVs. G.D.G. and R.L. performed RNA-seq. M.D.P. coordinated and supervised research, analyzed the data, and wrote the manuscript with input from all authors.

ACKNOWLEDGMENTS

We thank Luigi Naldini for sharing LV constructs, Ioannis Xenarios for support with bioinformatic studies, and M. Luisa Iruela-Arispe for help with the Matrigel plug experiments. This work was funded by Fonds National Suisse de la Recherche Scientifique (SNSF grant 31003A-143978), the National Center of Competence in Research (NCCR) in Molecular Oncology, the European Research Council (ERC Staring Grant Tie2+Monocytes), and Anna Fuller Fund (to M.D.P.). F.B. and M.I. were supported in part by the Swiss Federal Government through the State Secretariat for Education, Research and Innovation (SERI).

Received: May 8, 2014
Revised: July 1, 2014
Accepted: July 22, 2014
Published: August 21, 2014

REFERENCES

Amendola, M., Venneri, M.A., Biffi, A., Vigna, E., and Naldini, L. (2005). Coordinate dual-gene transgenesis by lentiviral vectors carrying synthetic bidirectional promoters. Nat. Biotechnol. *23*, 108–116.

Ameres, S.L., Martinez, J., and Schroeder, R. (2007). Molecular basis for target RNA recognition and cleavage by human RISC. Cell *130*, 101–112.

Ameres, S.L., Horwich, M.D., Hung, J.H., Xu, J., Ghildiyal, M., Weng, Z., and Zamore, P.D. (2010). Target RNA-directed trimming and tailing of small silencing RNAs. Science *328*, 1534–1539.

Baccarini, A., Chauhan, H., Gardner, T.J., Jayaprakash, A.D., Sachidanandam, R., and Brown, B.D. (2011). Kinetic analysis reveals the fate of a microRNA following target regulation in mammalian cells. Curr. Biol. *21*, 369–376.

Baek, D., Villén, J., Shin, C., Camargo, F.D., Gygi, S.P., and Bartel, D.P. (2008). The impact of microRNAs on protein output. Nature *455*, 64–71.

Baer, C., Squadrito, M.L., Iruela-Arispe, M.L., and De Palma, M. (2013). Reciprocal interactions between endothelial cells and macrophages in angiogenic vascular niches. Exp. Cell Res. *319*, 1626–1634.

Bartel, D.P. (2009). MicroRNAs: target recognition and regulatory functions. Cell *136*, 215–233.

Brown, B.D., and Naldini, L. (2009). Exploiting and antagonizing microRNA regulation for therapeutic and experimental applications. Nat. Rev. Genet. *10*, 578–585.

Brown, B.D., Gentner, B., Cantore, A., Colleoni, S., Amendola, M., Zingale, A., Baccarini, A., Lazzari, G., Galli, C., and Naldini, L. (2007). Endogenous microRNA can be broadly exploited to regulate transgene expression according to tissue, lineage and differentiation state. Nat. Biotechnol. *25*, 1457–1467.

Cesana, M., Cacchiarelli, D., Legnini, I., Santini, T., Sthandier, O., Chinappi, M., Tramontano, A., and Bozzoni, I. (2011). A long noncoding RNA controls muscle differentiation by functioning as a competing endogenous RNA. Cell *147*, 358–369.

Cifuentes, D., Xue, H., Taylor, D.W., Patnode, H., Mishima, Y., Cheloufi, S., Ma, E., Mane, S., Hannon, G.J., Lawson, N.D., et al. (2010). A novel miRNA processing pathway independent of Dicer requires Argonaute2 catalytic activity. Science *328*, 1694–1698.

Clausen, B.E., Burkhardt, C., Reith, W., Renkawitz, R., and Förster, I. (1999). Conditional gene targeting in macrophages and granulocytes using LysMcre mice. Transgenic Res. *8*, 265–277.

Denzler, R., Agarwal, V., Stefano, J., Bartel, D.P., and Stoffel, M. (2014). Assessing the ceRNA hypothesis with quantitative measurements of miRNA and target abundance. Mol. Cell *54*, 766–776.

Ellwanger, D.C., Büttner, F.A., Mewes, H.W., and Stümpflen, V. (2011). The sufficient minimal set of miRNA seed types. Bioinformatics *27*, 1346–1350.

Gentner, B., Schira, G., Giustacchini, A., Amendola, M., Brown, B.D., Ponzoni, M., and Naldini, L. (2009). Stable knockdown of microRNA in vivo by lentiviral vectors. Nat. Methods *6*, 63–66.

Gibbings, D.J., Ciaudo, C., Erhardt, M., and Voinnet, O. (2009). Multivesicular bodies associate with components of miRNA effector complexes and modulate miRNA activity. Nat. Cell Biol. *11*, 1143–1149.

Grimson, A., Farh, K.K., Johnston, W.K., Garrett-Engele, P., Lim, L.P., and Bartel, D.P. (2007). MicroRNA targeting specificity in mammals: determinants beyond seed pairing. Mol. Cell *27*, 91–105.

Guduric-Fuchs, J., O'Connor, A., Camp, B., O'Neill, C.L., Medina, R.J., and Simpson, D.A. (2012). Selective extracellular vesicle-mediated export of an overlapping set of microRNAs from multiple cell types. BMC Genomics *13*, 357.

Helwak, A., Kudla, G., Dudnakova, T., and Tollervey, D. (2013). Mapping the human miRNA interactome by CLASH reveals frequent noncanonical binding. Cell *153*, 654–665.

Hergenreider, E., Heydt, S., Tréguer, K., Boettger, T., Horrevoets, A.J., Zeiher, A.M., Scheffer, M.P., Frangakis, A.S., Yin, X., Mayr, M., et al. (2012). Atheroprotective communication between endothelial cells and smooth muscle cells through miRNAs. Nat. Cell Biol. *14*, 249–256.

Jakymiw, A., Lian, S., Eystathioy, T., Li, S., Satoh, M., Hamel, J.C., Fritzler, M.J., and Chan, E.K. (2005). Disruption of GW bodies impairs mammalian RNA interference. Nat. Cell Biol. *7*, 1267–1274.

Kosaka, N., Iguchi, H., Yoshioka, Y., Takeshita, F., Matsuki, Y., and Ochiya, T. (2010). Secretory mechanisms and intercellular transfer of microRNAs in living cells. J. Biol. Chem. *285*, 17442–17452.

Lai, E.C. (2002). Micro RNAs are complementary to 3′ UTR sequence motifs that mediate negative post-transcriptional regulation. Nat. Genet. *30*, 363–364.

Lewis, B.P., Burge, C.B., and Bartel, D.P. (2005). Conserved seed pairing, often flanked by adenosines, indicates that thousands of human genes are microRNA targets. Cell *120*, 15–20.

Liu, J., Valencia-Sanchez, M.A., Hannon, G.J., and Parker, R. (2005). MicroRNA-dependent localization of targeted mRNAs to mammalian P-bodies. Nat. Cell Biol. *7*, 719–723.

Manterola, L., Guruceaga, E., Gállego Pérez-Larraya, J., González-Huarriz, M., Jauregui, P., Tejada, S., Diez-Valle, R., Segura, V., Samprón, N., Barrena, C., et al. (2014). A small noncoding RNA signature found in exosomes of GBM patient serum as a diagnostic tool. Neuro-oncol. *16*, 520–527.

Martinez, F.O., Helming, L., and Gordon, S. (2009). Alternative activation of macrophages: an immunologic functional perspective. Annu. Rev. Immunol. *27*, 451–483.

Memczak, S., Jens, M., Elefsinioti, A., Torti, F., Krueger, J., Rybak, A., Maier, L., Mackowiak, S.D., Gregersen, L.H., Munschauer, M., et al. (2013). Circular RNAs are a large class of animal RNAs with regulatory potency. Nature *495*, 333–338.

Mittelbrunn, M., Gutiérrez-Vázquez, C., Villarroya-Beltri, C., González, S., Sánchez-Cabo, F., González, M.A., Bernad, A., and Sánchez-Madrid, F. (2011). Unidirectional transfer of microRNA-loaded exosomes from T cells to antigen-presenting cells. Nat Commun *2*, 282.

Montecalvo, A., Larregina, A.T., Shufesky, W.J., Stolz, D.B., Sullivan, M.L., Karlsson, J.M., Baty, C.J., Gibson, G.A., Erdos, G., Wang, Z., et al. (2012). Mechanism of transfer of functional microRNAs between mouse dendritic cells via exosomes. Blood *119*, 756–766.

Morelli, A.E., Larregina, A.T., Shufesky, W.J., Sullivan, M.L., Stolz, D.B., Papworth, G.D., Zahorchak, A.F., Logar, A.J., Wang, Z., Watkins, S.C., et al. (2004). Endocytosis, intracellular sorting, and processing of exosomes by dendritic cells. Blood *104*, 3257–3266.

Mullokandov, G., Baccarini, A., Ruzo, A., Jayaprakash, A.D., Tung, N., Israelow, B., Evans, M.J., Sachidanandam, R., and Brown, B.D. (2012). High-throughput assessment of microRNA activity and function using microRNA sensor and decoy libraries. Nat. Methods *9*, 840–846.

Nolte-'t Hoen, E.N., Buermans, H.P., Waasdorp, M., Stoorvogel, W., Wauben, M.H., and 't Hoen, P.A. (2012). Deep sequencing of RNA from immune cell-derived vesicles uncovers the selective incorporation of small non-coding RNA biotypes with potential regulatory functions. Nucleic Acids Res. *40*, 9272–9285.

Pigati, L., Yaddanapudi, S.C., Iyengar, R., Kim, D.J., Hearn, S.A., Danforth, D., Hastings, M.L., and Duelli, D.M. (2010). Selective release of microRNA species from normal and malignant mammary epithelial cells. PLoS ONE *5*, e13515.

Pillai, R.S. (2005). MicroRNA function: multiple mechanisms for a tiny RNA? RNA *11*, 1753–1761.

Poliseno, L., Salmena, L., Zhang, J., Carver, B., Haveman, W.J., and Pandolfi, P.P. (2010). A coding-independent function of gene and pseudogene mRNAs regulates tumour biology. Nature *465*, 1033–1038.

Ramachandran, S., and Palanisamy, V. (2012). Horizontal transfer of RNAs: exosomes as mediators of intercellular communication. Wiley Interdiscip Rev RNA *3*, 286–293.

Simons, M., and Raposo, G. (2009). Exosomes—vesicular carriers for intercellular communication. Curr. Opin. Cell Biol. *21*, 575–581.

Skog, J., Würdinger, T., van Rijn, S., Meijer, D.H., Gainche, L., Sena-Esteves, M., Curry, W.T., Jr., Carter, B.S., Krichevsky, A.M., and Breakefield, X.O. (2008). Glioblastoma microvesicles transport RNA and proteins that promote tumour growth and provide diagnostic biomarkers. Nat. Cell Biol. *10*, 1470–1476.

Squadrito, M.L., Pucci, F., Magri, L., Moi, D., Gilfillan, G.D., Ranghetti, A., Casazza, A., Mazzone, M., Lyle, R., Naldini, L., and De Palma, M. (2012). miR-511-3p modulates genetic programs of tumor-associated macrophages. Cell Rep *1*, 141–154.

Squadrito, M.L., Etzrodt, M., De Palma, M., and Pittet, M.J. (2013). MicroRNA-mediated control of macrophages and its implications for cancer. Trends Immunol. *34*, 350–359.

Stalder, L., Heusermann, W., Sokol, L., Trojer, D., Wirz, J., Hean, J., Fritzsche, A., Aeschimann, F., Pfanzagl, V., Basselet, P., et al. (2013). The rough endoplasmatic reticulum is a central nucleation site of siRNA-mediated RNA silencing. EMBO J. *32*, 1115–1127.

Tay, Y., Kats, L., Salmena, L., Weiss, D., Tan, S.M., Ala, U., Karreth, F., Poliseno, L., Provero, P., Di Cunto, F., et al. (2011). Coding-independent regulation of the tumor suppressor PTEN by competing endogenous mRNAs. Cell *147*, 344–357.

Tay, Y., Rinn, J., and Pandolfi, P.P. (2014). The multilayered complexity of ceRNA crosstalk and competition. Nature *505*, 344–352.

Turchinovich, A., Weiz, L., and Burwinkel, B. (2012). Extracellular miRNAs: the mystery of their origin and function. Trends Biochem. Sci. *37*, 460–465.

Valadi, H., Ekström, K., Bossios, A., Sjöstrand, M., Lee, J.J., and Lötvall, J.O. (2007). Exosome-mediated transfer of mRNAs and microRNAs is a novel mechanism of genetic exchange between cells. Nat. Cell Biol. *9*, 654–659.

Villarroya-Beltri, C., Gutiérrez-Vázquez, C., Sánchez-Cabo, F., Pérez-Hernández, D., Vázquez, J., Martin-Cofreces, N., Martinez-Herrera, D.J., Pascual-Montano, A., Mittelbrunn, M., and Sánchez-Madrid, F. (2013). Sumoylated hnRNPA2B1 controls the sorting of miRNAs into exosomes through binding to specific motifs. Nat Commun *4*, 2980.

Wen, J., Parker, B.J., Jacobsen, A., and Krogh, A. (2011). MicroRNA transfection and AGO-bound CLIP-seq data sets reveal distinct determinants of miRNA action. RNA *17*, 820–834.

Yates, L.A., Norbury, C.J., and Gilbert, R.J. (2013). The long and short of microRNA. Cell *153*, 516–519.

Cell Reports, Volume *8*

Supplemental Information

Endogenous RNAs Modulate MicroRNA Sorting to Exosomes and Transfer to Acceptor Cells

Mario Leonardo Squadrito, Caroline Baer, Frédéric Burdet, Claudio Maderna, Gregor D. Gilfillan, Robert Lyle, Mark Ibberson, and Michele De Palma

Supplemental Data

Supplemental Figures

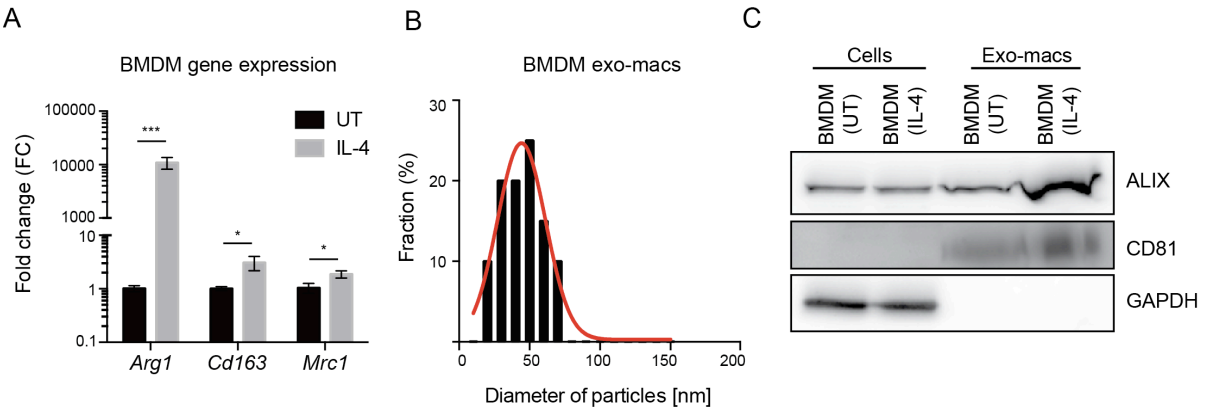

Figure S1. BMDMs polarization by IL-4 and secretion of exosomes, Related to Figure 1

A: TaqMan analysis of *Arg1*, *Cd163* and *Mrc1* (normalized to *B2m*) in IL-4–treated (IL-4) BMDMs versus untreated (UT) BMDMs. Data show mean values (± standard error of the mean (SEM), n=3). Statistical analysis by unpaired t-test.

B: Size distribution of BMDM-derived exo-macs, as determined by dynamic light scattering. Diameter (mean ± standard deviation) = 45.35±15.76 nm. Data represent 20 measurements of 4 biological samples.

C: Western blotting analysis of BMDMs, either untreated or stimulated with IL-4, and their exo-macs. ALIX and CD81 are exosomal markers. One representative experiment of 2 performed is shown.

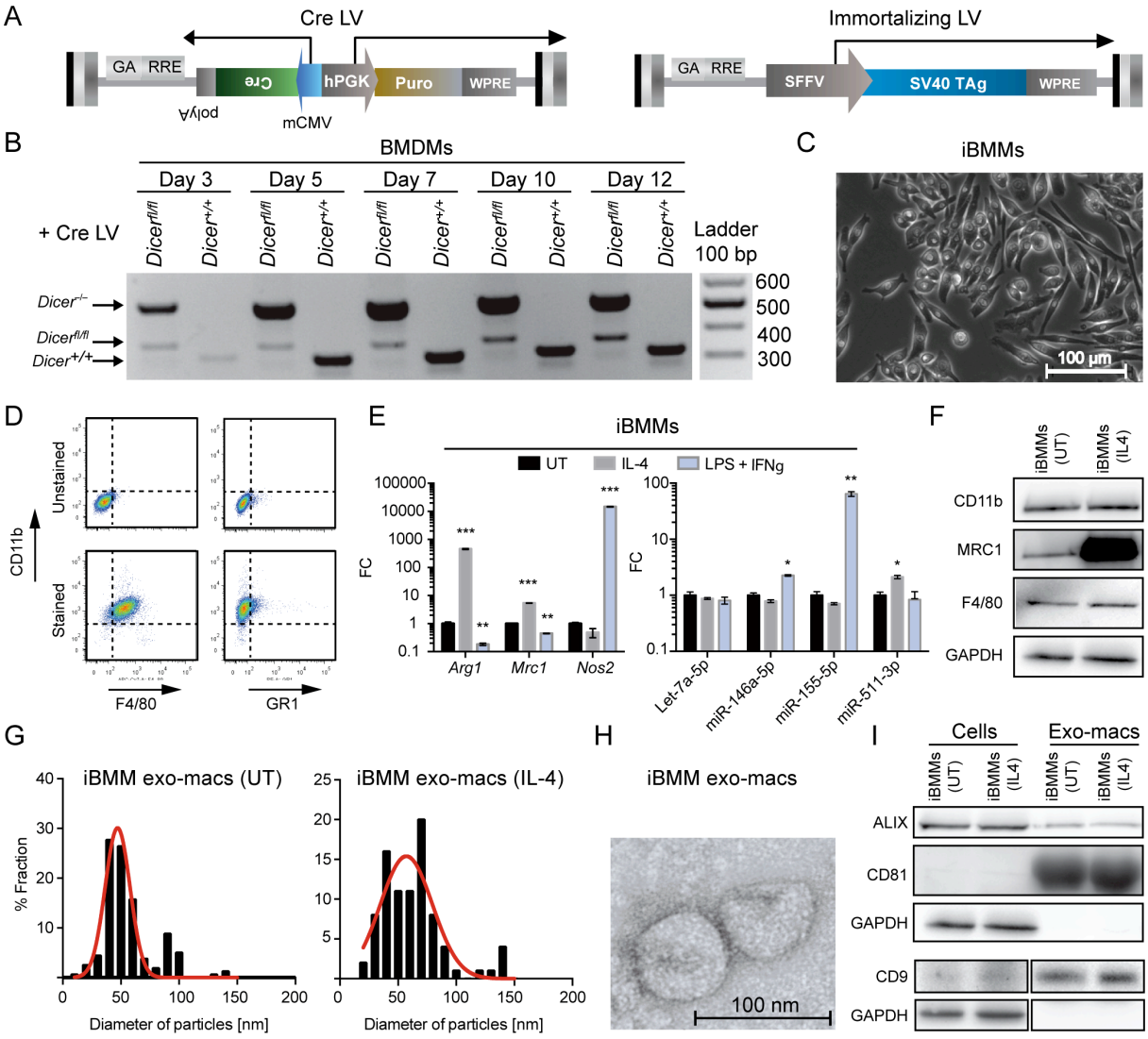

Figure S2. iBMMs are *bona fide* macrophages, secrete exosomes, and can be engineered to overexpress miR-511-3p or its artificial targets, Related to Figure 2

A: Schematic of the proviral LVs used to express Cre in BMDMs (left), or immortalize them (right).

B: PCR of *Dicer* in the genome of BMDMs isolated from *Dicer*$^{fl/fl}$ or *Dicer*$^{+/+}$ mice and transduced with a Cre-expressing LV on day 1. DNA was isolated from BMDMs after 3, 5, 7, 10 or 12 days of culture.

C: Bright-field microscopy of iBMMs.

D: Flow cytometry analysis of iBMMs. One representative experiment of several performed is shown.

E: TaqMan analysis of *Arg1*, *Mrc1* and *Nos2* (normalized to *Hprt*; left panel) and Let-7a-5p, miR-146a-5p, miR-155-5p and miR-511-3p (normalized to U6; right panel) in IL-4 or LPS+INFγ–treated (versus UT) iBMMs. Data show mean fold change (FC) values (±SEM,

n=2) normalized to untreated BMDMs (UT; black bar). Statistical analysis by unpaired Student's t-test.

F: Western blotting analysis of iBMMs, either untreated or stimulated with IL-4. ALIX, CD81 and CD9 are exosomal markers. One representative experiment of 2 performed is shown.

G: Size distribution analysis by dynamic light scattering of exo-macs obtained from UT (n=157 measurements of 5 biological samples) or IL-4–treated iBMMs (n=87 measurements of 5 biological samples).

H: Transmission electron microscopy of iBMM-derived exo-macs.

I: Western blotting analysis of iBMMs, either UT or IL-4–treated, and their exo-macs. Two representative experiments of 3 performed are shown.

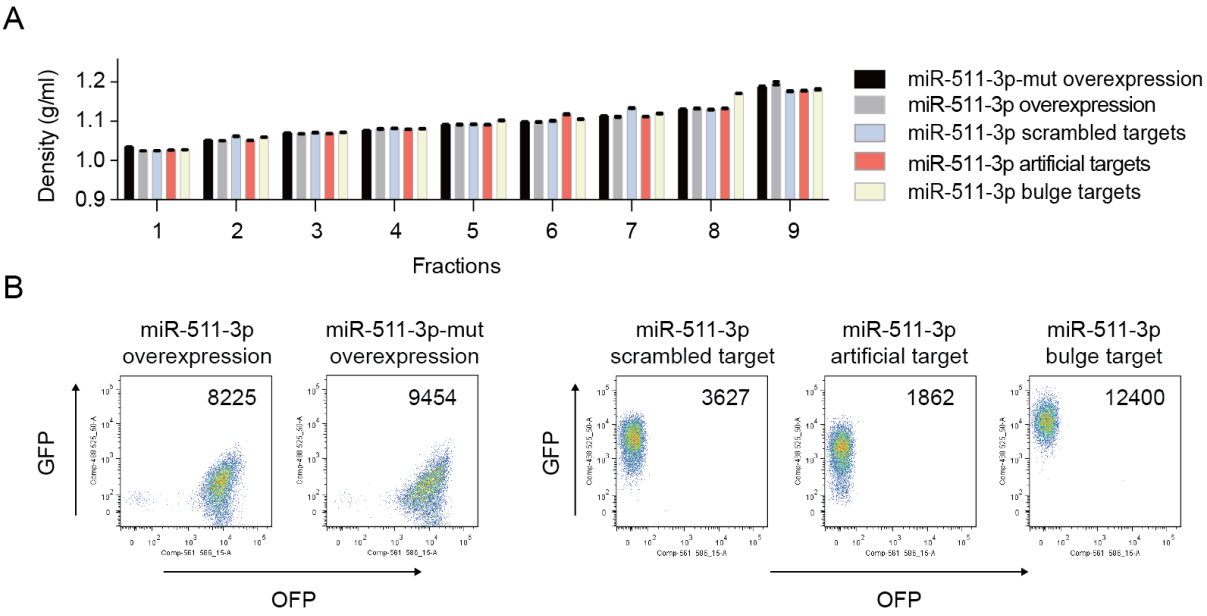

Figure S3. Subcellular fractionation of iBMMs, Related to Figure 3

A: Subcellular fractionation of iBMMs transduced with the indicated LVs. The histograms show the density (mean ± SEM, n=3 technical replicates) of the 9 fractions collected following ultracentrifugation of the OptiPrep gradient. One representative experiment of several performed is shown.

B: Flow cytometry analysis of iBMMs transduced with the indicated LVs. The mean fluorescence intensity (MFI) of OFP (left panel) or GFP (right panel) is indicated in each plot.

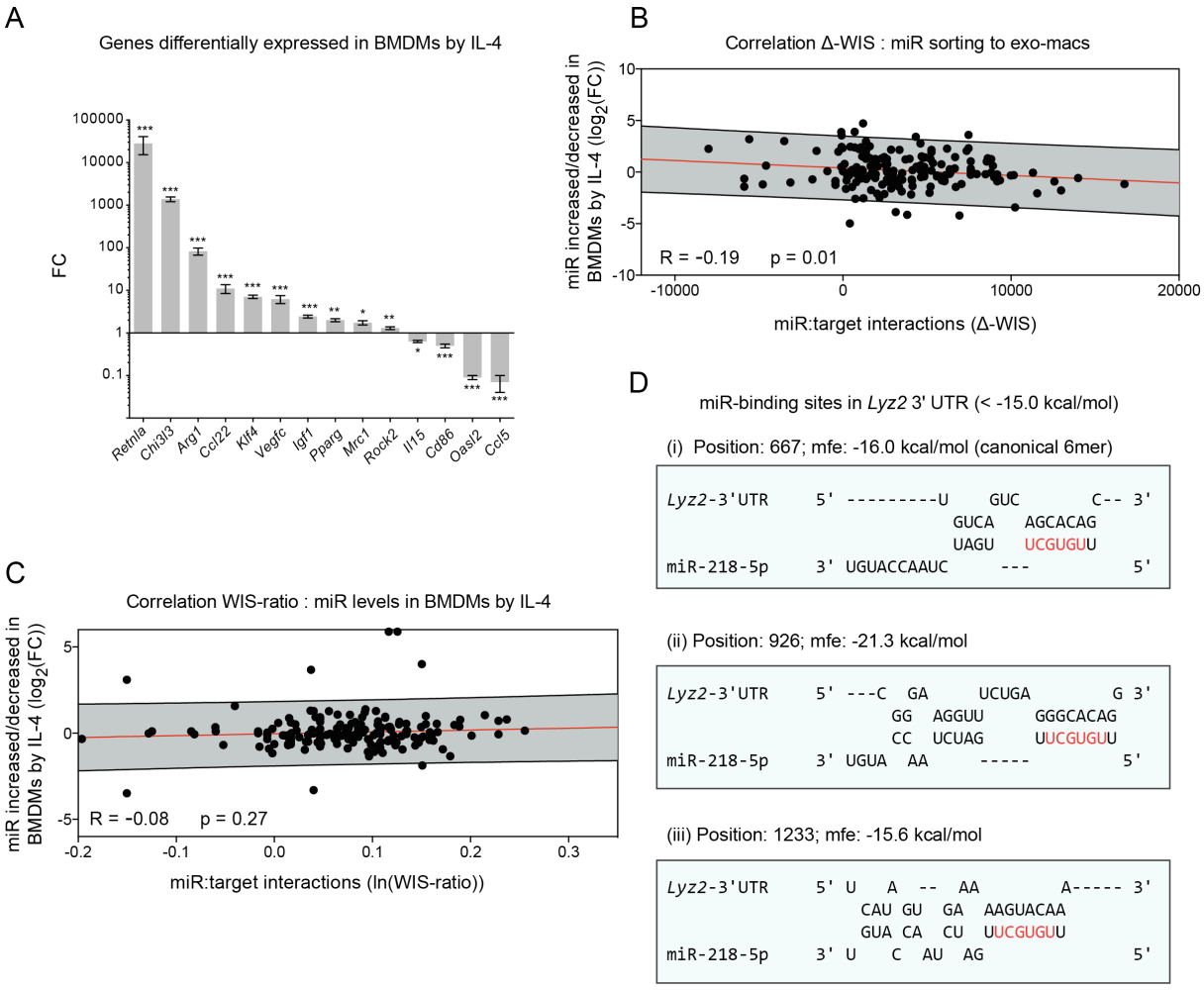

Figure S4. Gene-transcript levels modulate miR sorting to exo-macs, Related to Figure 4

A: Selected genes differentially expressed in BMDMs upon IL-4 treatment, analyzed by RNA-Seq. Data show fold-change (FC) versus UT BMDMs ($FC=2^{-\Delta Ct}$, mean ± SEM, n=3). Statistical analysis of the data by moderated t-statistics adjusted for false discovery rate (FDR).

B: Correlation between the Δ-WIS, measuring the absolute increase or decrease (Δ) of the WIS of each miR in IL-4–treated versus UT BMDMs, and miR sorting to exo-macs following IL-4 treatment (versus BMDMs; shown as log_2(FC) of miR levels). The gray area identifies 95% of the events (95% prediction band). Note that the majority of the Δ-WIS values are >0, indicating that the absolute levels of transcripts upregulated by IL-4 changed to a greater extent than did those downregulated by IL-4.

C: Correlation between the WIS-ratio (shown as ln(WIS-ratio)) and miR levels (shown as log_2(FC) of miR levels) in IL-4–treated versus UT BMDMs. The grey area identifies 95% of

the events (95% prediction band).

D: Target sites for miR-218-3p in the *Lyz2* 3'-UTR (minimal free energy, mfe ≤15.0 kcal/mol), as predicted by RNAhybrid. The seed sequence of the miR is indicated in red. (i) shows a canonical 6mer interaction; (ii-iii) show non-canonical interactions.

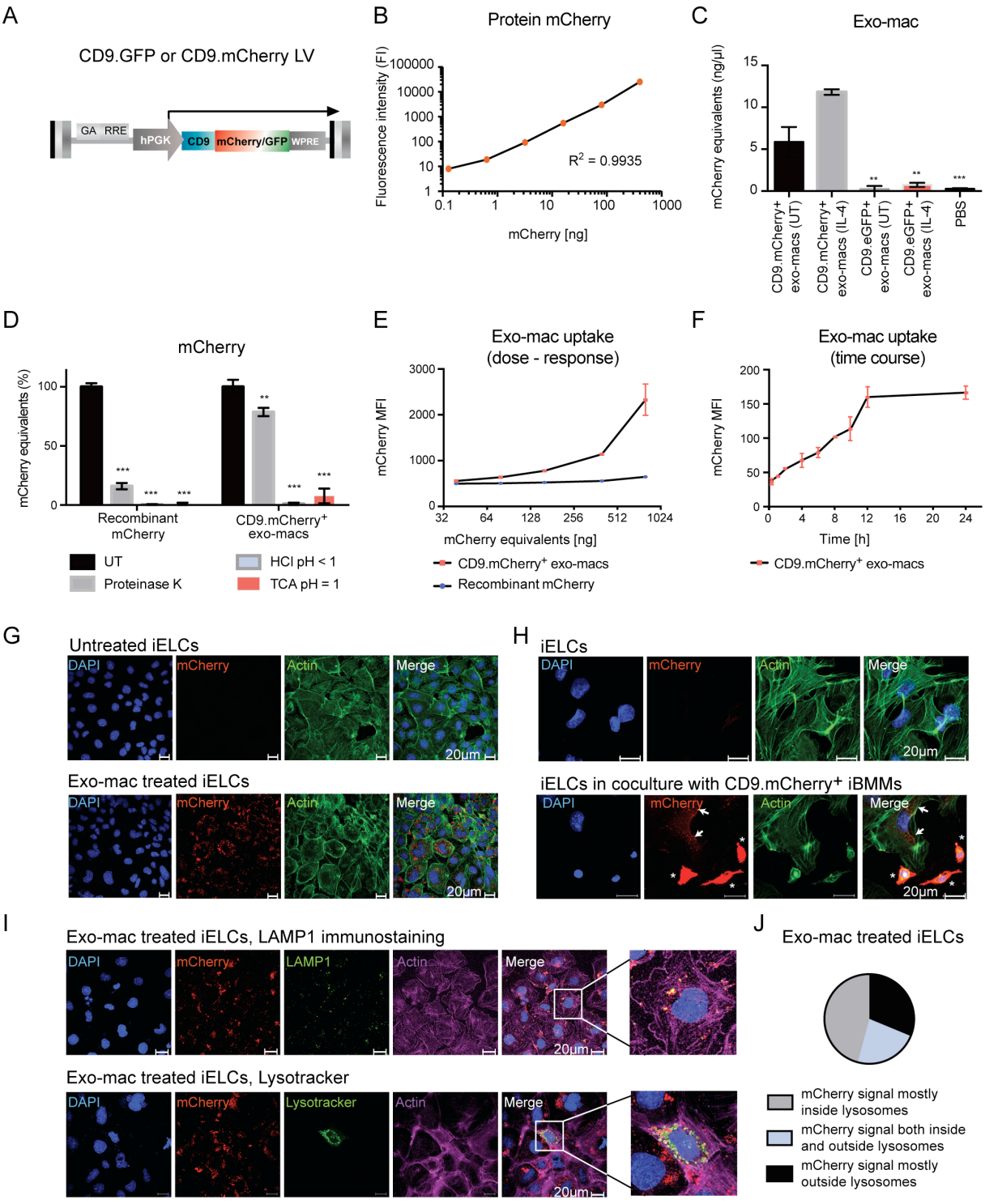

Figure S5. Exo-mac transfer from iBMMs to iELCs, and exo-mac colocalization with lysosomes, Related to Figure 5

A: Schematic of the proviral LV used to express the fusion proteins CD9-mCherry or CD9-GFP.

B: Relationship between mCherry protein and fluorescence intensity (FI) as shown by a standard curve obtained by measuring the FI of increasing doses of recombinant mCherry protein (n=3, R^2 = 0.9935).

C: mCherry protein equivalents for different exo-mac preparations, calculated using the standard curve shown in (B). Data show mean values of protein equivalents (± SEM, n=2). Statistical analysis by unpaired t-test.

D: mCherry protein equivalents for recombinant mCherry protein or CD9.mCherry$^+$ exo-macs after the indicated treatments. Data are shown as percentage (mean values ± SEM, n=3) of mCherry equivalents in UT. Statistical analysis by 2-way ANOVA with Bonferroni's multiple comparisons test.

E: Dose-response of mCherry MFI following treatment of iELCs, as indicated. Data show mean values (± SEM, n=2).

F: Time-course of mCherry MFI following treatment of iELCs, as indicated. Data show mean values (± SEM, n=2).

G-H: mCherry immunostaining (red), actin staining by phalloidin (green), and nuclear staining by DAPI (blue), of iELCs treated with exo-macs isolated from CD9.mCherry$^+$ iBMMs (G) or cocultured with CD9.mCherry$^+$ iBMMs (H). The asterisks indicate mCherry$^+$ macrophages; arrows indicate internalized mCherry$^+$ exo-macs. Representative images are shown from 7 (G) and 2 (H) independent experiments.

I: mCherry (red) immunostaining, LAMP1 (green, top panel) immunostaining or direct fluorescence of LAMP1-GFP Lysotracker (green, bottom panel), and nuclear staining by DAPI (blue), of iELCs treated with exo-macs isolated from CD9.mCherry$^+$ iBMMs. Images show colocalization between mCherry and lysosomes in some of the iELCs. Images are representative of many acquired from 2 independent experiments. For quantification, see J.

J: Proportion of iELCs that display mCherry signal within lysosomes, as assessed by Lysotracker. The analysis was performed on 50 cells that showed Lysotracker-positive staining.

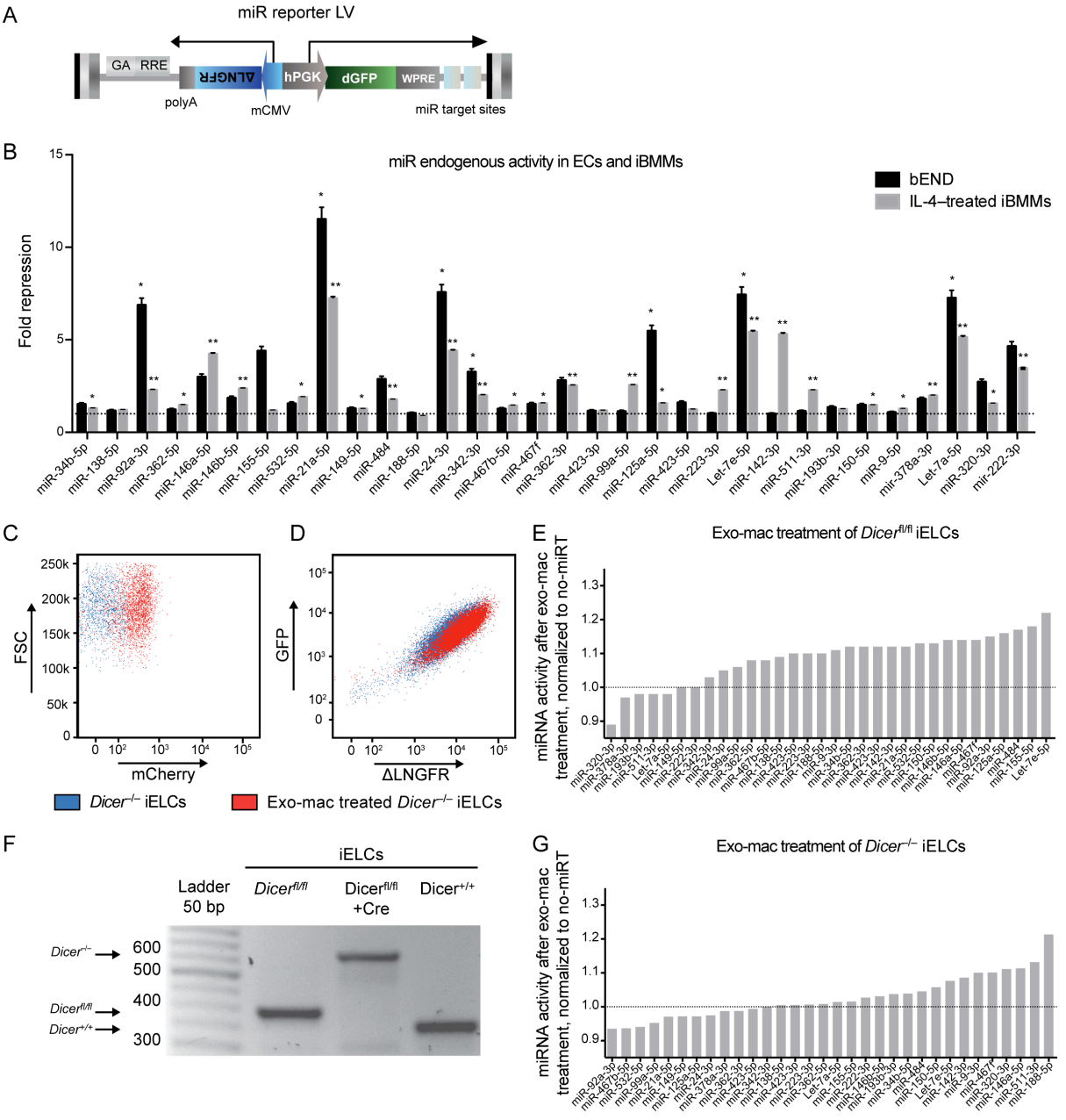

Figure S6. Transfer of miR activity to iELCs by exo-macs or coculture with iBMMs, Related to Figure 6

A: Schematic of the proviral LV used to measure miR activity (miR reporter LV).

B: Endogenous miR activity in bENDs (n=4) and IL-4–treated iBMMs (n=2) measured by miR reporter LVs, shown as GFP fold-repression normalized to iELCs transduced with a no-miRT control LV. Data show mean values (± SEM). Statistical analysis by adjusted one-sample t-test.

C-D: Flow cytometry analysis of mCherry (C) or GFP and ΔLNGFR (D) fluorescence in *Dicer*$^{-/-}$ iELCs left untreated or treated with exo-macs isolated from CD9.mCherry^{+} iBMMs. Panel C shows a shift in mCherry fluorescence (blue to red) following exo-mac treatment of

iELCs. Panel D shows slight GFP repression (blue to red) following exo-mac treatment of iELCs that were previously transduced with a miR reporter LV containing target sequences for miR-142-3p. For quantification of the data, see panel G.

E: miR activity in *Dicer*$^{fl/fl}$ iELCs after exo-macs treatment (versus untreated; n=2), measured by miR reporter LVs (normalized to a no-miRT LV).

F: PCR of *Dicer* in the genome of iELCs isolated from *Dicer*$^{fl/fl}$ or *Dicer*$^{+/+}$ mice and transduced, where indicated, with a Cre-expressing LV.

G: miR activity in *Dicer*$^{-/-}$ iELCs after exo-mac treatment (versus untreated; n=2), measured by miR reporter LVs (normalized to a no-miRT LV).

Supplemental Tables

Table S1. Normalized C_t values of miRs with at least 2 out of 3 determinations in all samples (178 miRs in total), Related to Figure 1

Table S2. (A) miRs increased/decreased in BMDMs by IL-4. (B) miRs increased/decreased in exo-macs by IL-4. (C) miRs increased/decreased in exo-macs versus BMDMs (untreated). (D) miRs increased/decreased in exo-macs versus BMDMs (IL-4–treated). (E) miRs increased/decreased in exo-macs versus BMDMs, IL-4–dependent, Related to Figure 1

Table S3. Genes differentially expressed in BMDMs by IL-4 treatment, Related to Figure 4

Supplemental Experimental Procedures

Mice

C57BL/6 and Swiss *nu*/*nu* mice were purchased from Charles River Laboratory (L'Arbresle, France). BM cells and heart tissue of *Dicer*$^{fl/fl}$ mice (Cobb et al., 2005) were a gift of Freddy Radtke (ISREC, EPFL). BM cells of *Lyz2*.Cre mice (Clausen et al., 1999) were a gift of Tatiana Petrova (UNIL). All mice employed in this study were maintained in a pathogen-free barrier animal facility in accord with Swiss regulations for the care and use of mice in experimental research. All procedures were performed according to protocols approved by the Veterinary Authorities of the Canton Vaud according to the Swiss Law.

Lentiviral vector (LV) construction

Third generation lentiviral vector particles pseudotyped with the vesicular stomatitis virus (VSV)-G envelope were used to express miR reporter LVs, miR-511-3p, miR-511-3p target sequences, Cre recombinase, CD9-fusion proteins and large-T antigen.

miR reporter LVs

miR reporter LVs used in this study were generated by introducing 2 sequences with perfect complementarity to specific miRs (miRT sequences) downstream to a destabilized-GFP (dGFP) transgene expressed from a bidirectional LV also encoding for a ΔLNGFR transgene (ΔLNGFR←→dGFP LV) (Amendola et al., 2005). Individual miRT sequences were designed based on miR sequences obtained from the miR registry (http://microrna.sanger.ac.uk/). In order to generate a large panel of miR reporter LVs, we first designed and synthetized (GeneArt, Lifetechnologies) 3 synthetic DNA sequences, termed Set-A, Set-B and Set-C, each containing tandem miRT sequences for the selected miRs (miRT.1 to 12) in either sense (S_miRT) or anti-sense (AS_miRT) orientation. Consensus sites for restriction enzymes (all from New England BioLabs) were inserted between 2 consecutive miRT sequences.

Set-A and Set-B

XbaI-S_miRT.1-XmaI-AS_miRT.2-NheI-S_miRT.3-AgeI-S_miRT.4-kpnI-AS_miRT.5-SpeI-S_miRT.6-XmaI-S_miRT.7-kpnI-AS_miRT.8-XbaI-S_miRT.9-AgeI-AS_miRT.10-AvrII-S_miRT.11-kpnI-AS_miRT.12-NheI

Set-C

XbaI-S_miRT.1-XmaI-AS_miRT.2-XbaI-S_miRT.3-AgeI-S_miRT.4-kpnI-AS_miRT.5-SpeI-S_miRT.6-XmaI-S_miRT.7-kpnI-AS_miRT.8-NheI-S_miRT.9-AgeI-AS_miRT.10-AvrII-

S_miRT.11-kpnI-AS_miRT.12-XbaI

Individual miRT sequences were obtained by digesting the set sequences with specific combinations of 2 restriction enzymes. The resulting fragments were then cloned into the bidirectional LV, previously digested with XbaI/XmaI, XmaI/KpnI or XbaI/KpnI, according to the restriction sites flanking the miRT fragment. miRT sequences are listed below.

Position	Set-A	Set-B	Set-C
miRT.1	Aborted	mmu-miR-188-5p	mmu-miR-223-3p
miRT.2	mmu-miR-34b-5p	Aborted	mmu-Let-7e-5p
miRT.3	mmu-miR-138-5p	mmu-miR-24-3p	mmu-miR-142-3p
miRT.4	mmu-miR-92a-3p	Aborted	mmu-miR-511-3p
miRT.5	mmu-miR-362-5p	mmu-miR-342-3p	mmu-miR-193b-3p
miRT.6	mmu-miR-146a-5p	mmu-miR-467b-5p	Aborted
miRT.7	mmu-miR-146b-5p	mmu-miR-467f	mmu-miR-150-5p
miRT.8	mmu-miR-155-5p	mmu-miR-362-3p	mmu-miR-9-5p
miRT.9	mmu-miR-532-5p	mmu-miR-423-3p	mmu-miR-378a-3p
miRT.10	mmu-miR-21a-5p	mmu-miR-99a-5p	mmu-Let-7a-5p
miRT.11	mmu-miR-149-5p	mmu-miR-125a-5p	mmu-miR-320-3p
miRT.12	mmu-miR-484	mmu-miR-423-5p	mmu-mir-222-3p

The sequences of set-A, set-B and set-C are reported below:

>Set-A

TCTAGAAGTAGTGCTTTCTACTTTATGAATTAGTAGTGCTTTCTACTTTATGCCCGGGTAGGCAGT
GTAATTAGCTGATTGTAATTTAGGCAGTGTAATTAGCTGATTGTGCTAGCCGGCCTGATTCACAAC
ACCAGCTAATTCGGCCTGATTCACAACACCAGCTACCGGTCAGGCCGGGACAAGTGCAATAAATT
CAGGCCGGGACAAGTGCAATAGGTACCAATCCTTGGAACCTAGGTGTGAATAATTAATCCTTGGA
ACCTAGGTGTGAATACTAGTAACCCATGGAATTCAGTTCTCAAATTAACCCATGGAATTCAGTTCT
CACCCGGGAGCCTATGGAATTCAGTTCTCAAATTAGCCTATGGAATTCAGTTCTCAGGTACCTTAA
TGCTAATTGTGATAGGGGTAATTTTAATGCTAATTGTGATAGGGGTTCTAGAACGGTCCTACACTC
AAGGCATGAATTACGGTCCTACACTCAAGGCATGACCGGTTAGCTTATCAGACTGATGTTGAAAT
TTAGCTTATCAGACTGATGTTGACCTAGGGGGAGTGAAGACACGGAGCCAGAAATTGGGAGTGA
AGACACGGAGCCAGAGGTACCTCAGGCTCAGTCCCCTCCCGATAATTTCAGGCTCAGTCCCCTC
CCGATGCTAGC

>Set-B

TCTAGACCCTCCACCATGCAAGGGATGAATTCCCTCCACCATGCAAGGGATGCCCGGGCTGGCC
CTCTCTGCCCTTCCGTAATTCTGGCCCTCTCTGCCCTTCCGTGCTAGCCTGTTCCTGCTGAACTG

AGCCAAATTCTGTTCCTGCTGAACTGAGCCAACCGGTTCACATGTACATGTACACACACAAATTTC
ACATGTACATGTACACACACAGGTACCTCTCACACAGAAATCGCACCCGTAATTTCTCACACAGAA
ATCGCACCCGTACTAGTCATATACATGCAGGCACTTACAATTCATATACATGCAGGCACTTACCCC
GGGTGTAGGTGTGTGTGTGTATATAATTTGTAGGTGTGTGTGTGTATATGGTACCAACACACCTG
TTCAAGGATTCAAATTAACACACCTGTTCAAGGATTCATCTAGAACTGAGGGGCCTCAGACCGAG
CTAATTACTGAGGGGCCTCAGACCGAGCTACCGGTAACCCGTAGATCCGATCTTGTGAATTAACC
CGTAGATCCGATCTTGTGCCTAGGTCACAGGTTAAAGGGTCTCAGGGAAATTTCACAGGTTAAAG
GGTCTCAGGGAGGTACCTGAGGGGCAGAGAGCGAGACTTTAATTTGAGGGGCAGAGAGCGAGA
CTTTGCTAGC

>Set-C

TCTAGATGGGGTATTTGACAAACTGACAAATTTGGGGTATTTGACAAACTGACACCCGGGTGAGG
TAGGAGGTTGTATAGTTAATTTGAGGTAGGAGGTTGTATAGTTTCTAGAATCCATAAAGTAGGAAA
CACTACAAATTATCCATAAAGTAGGAAACACTACAACCGGTATCCTGTCTTTTGCTACACATTAATT
ATCCTGTCTTTTGCTACACATTGGTACCAACTGGCCCACAAAGTCCCGCTAATTAACTGGCCCAC
AAAGTCCCGCTACTAGTGTGCCTCACCTCAGCCATTGAAATTGTGCCTCACCTCAGCCATTGACC
CGGGCACTGGTACAAGGGTTGGGAGAAATTCACTGGTACAAGGGTTGGGAGAGGTACCTCTTTG
GTTATCTAGCTGTATGAAATTTCTTTGGTTATCTAGCTGTATGAGCTAGCCCTTCTGACTCCAAGT
CCAGTAATTCCTTCTGACTCCAAGTCCAGTACCGGTTGAGGTAGTAGGTTGTATAGTTAATTTGAG
GTAGTAGGTTGTATAGTTCCTAGGTCGCCCTCTCAACCCAGCTTTTAATTTCGCCCTCTCAACCCA
GCTTTTGGTACCAGCTACATCTGGCTACTGGGTAATTAGCTACATCTGGCTACTGGGTTCTAGA

LVs for miR-511-3p overexpression

LVs to overexpress miR-511-3p, or its mutated form, were described previously (Squadrito et al., 2012). Briefly, we cloned a DNA fragment encompassing the miR-511 intronic sequence of the mouse *Mrc1* gene into a LV containing the spleen forming focus virus (SFFV) promoter and the orange fluorescent protein (OFP) reporter gene. A mutated form of miR-511-3p was obtained by introducing point mutations in the miR-511-3p sequence that did not affect the complementary miR-511-5p sequence (Squadrito et al., 2012).

LVs for the overexpression of target sequences for miR-511-3p

LVs to overexpress artificial target sequences for miR-511-3p are based on a SFFV.dGFP LV, which exploits the strong SFFV promoter to overexpress a dGFP transgene linked to 8 tandem sequences with complementarity to a given miR (Gentner et al., 2009). We implemented this vector design to generate 3 different LVs. To obtain a LV overexpressing artificial target sequences for miR-511-3p, we introduced 8 tandem sequences with perfect complementarity to miR-511-3p into the 3'-UTR of the SFFV.dGFP cassette. To obtain a LV overexpressing bulge target sequences for miR-511-3p, we introduced 8 tandem copies with partial complementarity to miR-511-3p (4 extra-nucleotides are present in the target

sequence that do not match the miR sequence; see below) into the 3'-UTR of the SFFV.dGFP cassette. To obtain a LV overexpressing scrambled target sequences for miR-511-3p, we introduced 8 tandem copies of a DNA sequence containing the same nucleotide composition of perfectly complementary target sequences for miR-511-3p, but ordered randomly, into the 3'-UTR of the SFFV.dGFP cassette. All the DNA sequences were purchased from GeneArt, Life Technologies, and cloned by using XbaI and KpnI restriction sites. In the below sequences, bold/underlined nucleotides indicate complementarity to miR-511-3p; italic/underlined nucleotides indicate the scrambled miR-511-3p target sequence.

>artificial_target_miR-511-3p

TCTAGA**ATCCTGTCTTTTGCTACACATT**GCGC**ATCCTGTCTTTTGCTACACATT**GCGC**ATCCTGTCTTTTGCTACACATT**GCGC**ATCCTGTCTTTTGCTACACATT**GCGC**ATCCTGTCTTTTGCTACACATT**GCGC**ATCCTGTCTTTTGCTACACATT**GCGC**ATCCTGTCTTTTGCTACACATT**GGTACC

>bulge-artificial_target_miR-511-3p

TCTAGA**ATCCTGTCTTTTG**ATCG**CTACACATT**GGCC**ATCCTGTCTTTTG**ATGG**CTACACATT**GATC**ATCCTGTCTTTTG**AACG**CTACACATT**GGAC**ATCCTGTCTTTTG**AAGG**CTACACATT**GAAC**ATCCTGTCTTTTG**AACG**CTACACATT**GTCC**ATCCTGTCTTTTG**AAGG**CTACACATT**GATC**ATCCTGTCTTTTG**AAAG**CTACACATT**GGTC**ATCCTGTCTTTTG**ACAG**CTACACATT**GGTACC

>scr-artificial_target_miR-511-3p

TCTAGA*CATTTCCTATCCTTATGCTTAG*GCGC*CATTTCCTATCCTTATGCTTAG*CCGG*CATTTCCTATCCTTATGCTTAG*GCAT*CATTTCCTATCCTTATGCTTAG*ACGCGT*CATTTCCTATCCTTATGCTTAG*GTCT*CATTTCCTATCCTTATGCTTAG*CCGC*CATTTCCTATCCTTATGCTTAG*CGGC*CATTTCCTATCCTTATGCTTAG*GGTACC

LVs for the overexpression of natural target sequences for miR-511-3p

Natural target sequences for miR-511-3p were obtained from the *Rock2* 3'-UTR, as described previously (Squadrito et al., 2012). Briefly, to express the fragment of the *Rock2* 3'-UTR containing miR-511-3p target sequences, we generated by DNA synthesis (GeneArt, Invitrogen) a 500 nt long DNA fragment corresponding to the mouse *Rock2* 3'-UTR and encompassing a "core" UTR region containing 3 target sites for miR-511-3p. We also generated a mutated *Rock2* 3'-UTR fragment; point mutations were inserted that abrogated miR-511-3p seed/target mRNA interactions. We cloned the synthetic DNA fragment in ΔLNGFR←→GFP bidirectional LV downstream to the GFP expression cassette (Squadrito et al., 2012).

LVs to express CD9.mCherry and CD9.GFP fusion proteins

LVs expressing CD9.mCherry and CD9.GFP fusion proteins were obtained by cloning a 676 nt long CD9 coding sequence downstream to the human phosphoglycerate kinase (hPGK) promoter and upstream to either the mCherry or GFP cDNA. The CD9 coding sequence was retrotranscribed from BMDMs using the following primers, containing BamHI and AgeI restriction sites:

>FW_CD9
AAAAAAGGATCCATGCCGGTCAAAGGAGGTAGCAAG
>RV_CD9
AAAAAAAGATCTACCGGTACCATTTCTCGGCTCCTGCGG

LV to express the Cre recombinase

The Cre LV was generated by replacing the ΔLNGFR and the GFP DNA sequences of a ΔLNGFR←→GFP bidirectional LV (Amendola et al., 2005), with Cre and puromycin resistance (Puro) coding sequences, respectively. The Cre cDNA was inserted in the LV in place of ΔLNGFR by using AfeI and NheI restriction enzymes. The Puro coding sequence was obtained from an hPGK.Puro plasmid (a gift from I. Barde and D. Trono, EPFL) and inserted in the LV in place of GFP by using the Asc1 and KpnI restriction enzymes.

LV to immortalize macrophages and endothelial cells

The SV40 large T Antigen (TAg) coding sequence (a gift from D. Trono, EPFL) was cloned in a SFFV promoter-containing LV (Squadrito et al., 2012) by using BamHI and SalI restriction enzymes. The resultant LV was termed SFFV.TAg LV.

LV production

Vesicular stomatitis virus (VSV)-pseudotyped, third-generation LVs were produced by transient four-plasmid cotransfection into 293T cells and concentrated by ultracentrifugation, as described (De Palma and Naldini, 2002). Expression titers of LVs expressing fluorescent proteins were determined on 293T cells by limiting dilution; titers of LVs not expressing fluorescent proteins were determined on 293T cells by TaqMan analysis of vector sequences, as described (De Palma et al., 2008). LV titers of 293T conditioned medium (before ultracentrifugation) ranged from 10^6 to 10^7 transducing units/ml. For some applications, 293T conditioned medium was ultracentrifuged to obtain high-titer LVs, as described (De Palma et al., 2008). LV stocks were stored at –80°C.

LV transduction

Cells were transduced with LV doses ranging from 10^3 to 10^7 transducing units (TU)/ml, depending on the cell type. Primary bone marrow (BM)-derived macrophages (BMDMs) were transduced with LV doses ranging from 10^6 to 10^7 TU/ml. In dose-response experiments, immortalized BM macrophages (iBMMs) were transduced with LV doses ranging from 10^3 to 10^7. Immortalized endothelial-like cells (iELCs) were transduced with LV doses ranging from 10^5 to 10^6 TU/ml. In some experiments, sequential transduction was performed by (i) transducing the cells with the first LV; (ii) washing and replating the cells; and (iii) transducing the cells with the second LV (superinfection) on day 5–7 after the first transduction.

Cell lines

Human 293T, mouse bEND.3 cells and iELCs were maintained in Iscove's modified Dulbecco's medium (IMDM; Sigma) supplemented with 10% fetal bovine serum (FBS; Promega), 2 mM L-glutamine (Amimed) and a combination of 50 units/ml penicillin and 50 µg/ml streptomycin (Gibco). iBMMs were maintained in IMDM with 20% FBS, penicillin-streptomycin and glutamine, and 50 ng/mL CSF-1. To isolate exosomes, cells were cultured in serum-free, macrophage SFM medium (Life Technologies) supplemented as described below.

Bone marrow-derived macrophages (BMDMs)

BM cells were obtained by flushing the long bones of 8-week old female C57BL/6 or *Dicer*$^{fl/fl}$ C57BL/6 mice. BM cells were then were plated in macrophage SFM medium (Life Technologies) supplemented with penicillin-streptomycin and CSF-1 (Peprotech, 100 ng/ml) and cultured for one week to allow macrophage differentiation. In some experiments, BMDMs were polarized by adding IL-4 to the medium (40 ng/ml, Peprotech) for 72 h. In order to transduce BMDMs with LVs, BM cells were plated and non-adherent cells transduced on day 1. Transduced cells were then cultured as described above.

Immortalization of macrophages and endothelial cells (ECs)

Immortalized bone-marrow macrophages (iBMMs)

BM cells were obtained by flushing the long bones of 8-week old female *Dicer*$^{fl/fl}$ or *Dicer*$^{+/+}$ C57BL/6 mice. On day 1 post-plating, non-adherent BM cells were transduced with a LV expressing the SV40 large T antigen (SFFV.Tag LV; see above). Macrophages were cultured in macrophage SFM medium (Life Technologies) supplemented with CSF-1 (50 ng/ml) for 2 weeks before selection of bona fide macrophages using F4/80-coated microbeads (Dynabeads, Life technologies). Single *Dicer*$^{fl/fl}$ and *Dicer*$^{+/+}$ clones were then

obtained by limiting dilution that expressed F4/80, CD11b, but not Gr1. One *Dicer*$^{fl/fl}$ clone was selected and used for subsequent experiments.

Immortalized endothelial-like cells (iELCs)

Endothelial cells were isolated from the heart of *Dicer*$^{fl/fl}$ or *Dicer*$^{+/+}$ C57BL/6 mice using CD31-coated microbeads (Dynabeads, Life technologies). Heart-derived, primary endothelial cells were transduced with the SFFV.Tag LV and single clones (either *Dicer*$^{fl/fl}$ or *Dicer*$^{+/+}$) obtained by limiting dilution. One *Dicer*$^{fl/fl}$ clone was selected and used for subsequent experiments. This clone expressed low-level EC genes, including *Flt1*, *c-kit* and *Sca1*, by TaqMan or flow cytometry, respectively.

Dicer deletion in iBMMs and iELCs

In order to obtain *Dicer*$^{-/-}$ iBMMs, we transduced *Dicer*$^{fl/fl}$ iBMMs with the Cre/Puro-expressing bidirectional LV and cultured them in puromycin for 10 days before replacing the medium for subsequent exo-mac isolation. *Dicer*$^{-/-}$ iBMMs could not be maintained in culture for more than 2-3 weeks, likely due to the inability of *Dicer*-deficient macrophages to survive in culture (data not shown). *Dicer*$^{-/-}$ iELCs were obtained by transducing *Dicer*$^{fl/fl}$ iELCs with the Cre/Puro-expressing bidirectional LV. After puromycin treatment, several *Dicer*-deficient clones could be isolated that could be expanded in culture for several weeks. One *Dicer*$^{-/-}$ iELC clone was selected and used for subsequent experiments.

Exosome isolation

In order to isolate macrophage-derived exosomes (exo-macs), BMDMs and iBMMs were cultured in serum-free medium (SFM medium; Life Technologies). In coculture experiments (e.g., iBMMs with ECs), culture medium was supplemented with FBS previously depleted of exosomes by ultracentrifugation at 134'000xg for 6 h. In order to isolate exo-macs, we employed two different techniques:

(i) ExoQuick TC (System Biosciences). Briefly, the cell culture medium was replaced 3 days before exo-mac isolation using fresh SFM medium. Medium was centrifuged at 500xg for 5 min; 2000xg for 5 min; and finally at 4600xg for 20 min at 4°C to remove cells and debris. The pellet was then resuspended in ExoQuick (1 ml for 5 ml of starting medium). Following overnight incubation, the mixture was centrifuged at 1500xg for 30 min and the pellet resuspended either in PBS, RIPA buffer, or Qiazol depending on the application. BMDM-derived exo-macs were consistently isolated by ExoQuick, which allows processing of small volumes of medium.

(ii) Ultracentrifugation. Briefly, medium was processed as described above (sequential centrifugation) and eventually ultracentrifuged at 134'000xg for 70 min at 4°C using a

Beckman ultracentrifuge. iBMM-derived exo-macs were consistently isolated by ultracentrifugation.

Exo-macs were used immediately or stored at –80°C.

Cell fractionation

iBMMs were transduced with LVs 3-4 weeks before lysis. Approximately 1-10^6 iBMMs were washed 3 times in PBS, once in 0.25 M sucrose/10 mM triethanolamine/10 mM acetic acid at pH 7.8, and finally resuspended in 1 ml of 0.25 M sucrose/10mM triethanolamine/1 mM EDTA/10 mM acetic acid at pH 7.8 with Complete Mini protease inhibitor (Roche), 4% ribonucleoside vanadyl complex (New England BioLabs), and 400 U RNAseOut (Invitrogen). Cell lysis was performed by 16 strokes of a Dounce homogenizer, and cell nuclei removed by centrifugation at 1500xg for 10 min at 4°C. Gradients were performed as described previously (Gibbings et al., 2009; Xia et al., 1998), with some adaptations. Iodixanol density media (OptiPrep, Axis-Shield) was used to fractionate cell compartments in different fractions. Briefly, 2.5 to 30% OptiPrep gradients were prepared in 0.25 M sucrose/10 mM triethanolamine/1 mM EDTA/10 mM acetic acid at pH 7.8 with Complete Mini protease inhibitor, 4% ribonucleoside vanadyl complex, and 400 U RNAseOut. Post-nuclear supernatants were then added on top of the OptiPrep gradients and centrifuged for 5 h at 90'000xg using a SW41 rotor and a Beckman ultracentrifuge. Nine fractions were obtained. The density of each fraction was analyzed by measuring the absorbance (335 nm) of 100 µl of each fraction using a Tecan Spectrophotometer. Densities were extrapolated from a standard curved based on 2.5 to 30% ionixadol. For RNA extraction and miR expression analysis, 200 µl for each fraction were lysed in 700 µl of Qiazol (Qiagen) and RNA extracted as indicated by the manufacturer. For protein extraction, see Western blotting below.

Protein extraction and Western blotting

Exo-macs

Exosomes obtained by ExoQuick or ultracentrifugation were lysed using RIPA lysis buffer (50 mM Tris-HCl, 150 mM NaCl, 1 mM EDTA pH 8.0, 1% Triton X-100, 1% Na-deoxycholate, 0.1% SDS supplemented with HALT protease and phosphatase inhibitor cocktail from Pierce). Protein concentration was measured by protein assays (Bio-Rad) and samples diluted in PBS/6x Laemmli buffer to equal concentration.

Cells

Cells were washed with PBS, collected by cell scrapers and directly lysed using RIPA lysis buffer. Protein concentration was measured by protein assays (Bio-Rad) and samples diluted in PBS/6x Laemmli buffer to equal concentration.

Subcellular fractions

One ml of each subcellular fraction was concentrated using StrataClean Resin (Agilent). Briefly, 30 µl of StrataClean Resin was added to each fraction and vortexed for 15 sec. The samples were then incubated for 1 h at 4°C with occasional mixing and washed twice with 1x PBS. Finally, 25 µl of 1x Laemmli buffer was added to each sample, which was then boiled at 95°C for 5 min, and directly loaded onto polyacrylamide gels.

Western blotting

Proteins (10-50 µg) were separated by electrophoresis on polyacrylamide gels and transferred onto PVDF blotting-membrane (Axon Lab). Ponceau staining (Sigma) was performed to confirm that the samples were loaded equally. The membranes were blocked in 5% nonfat dry milk in TBS-T (pH 7.6 with 0.5% Tween 20) for 1 h at room temperature. Primary antibodies were diluted in 5% nonfat dry milk in TBS-T and incubated on the membranes overnight at 4°C. Primary antibodies were then removed and the blots washed in TBS-T and incubated in horseradish peroxidase (HRP)-conjugated secondary antibodies (GE Healthcare) for 1 h at room temperature. Reactive proteins were visualized using ECL Western Blotting substrate (Pierce) and a Fusion FX7 device (Peqlab). We used the following primary antibodies: rabbit anti-GAPDH (Abcam), rabbit anti-CD11b (Abcam), rat anti-F4/80 (AbD Serotec), rabbit anti-CD81 (Sigma), rat anti-CD9 (AbD Serotec), mouse anti-ALIX (AbD Serotec), rabbit anti-AGO2 (Cell signaling), rabbit anti-LAMP1 (Abcam), rabbit anti-DCP1A (Abcam), rabbit anti-Calnexin (Abcam). The secondary antibodies were anti-rat, anti-rabbit, anti-mouse or anti-goat HRP-linked antibodies (GE Healthcare). For further information on antibodies, see below.

Exo-mac analysis

Transmission electron microscopy

Exo-macs (2 µl of preparation) were diluted 1:10 and applied on a formvar-carbon grid (Electron Microscopy Sciences, FCF-200-Cu) for 30 sec. The grid was subsequently washed with 3 drops of ultrapure water and stained with 2% uranyl acetate. Subsequently, the grids were washed with 6 drops of ultrapure water. Grids were immediately imaged on a Tecnai Spirit at 80kV transmission electron microscope.

Size analysis

Size analysis of exo-macs was performed by dynamic light scattering (DLS) using a Zetasizer Nano ZS (Malvern Instruments, UK) according to the manufacturer's instructions. Briefly, exo-macs (40 µl) were diluted in PBS to a final volume of 100 µl and loaded in 40 µl cuvettes (Malvern). Three-80 sequential acquisitions were performed for each exo-mac preparation.

Quantification

CD9.mCherry^{+} exo-macs were quantified by measuring mCherry fluorescence using a Tecan infinite2000 plate-reader (TECAN). The following parameters were used: excitation wavelength: 586 nm; emission wavelength: 625 nm; number of reads: 3. To standardize experiments whereby exo-macs were added to cell cultures to measure mCherry/miR transfer, we employed a standard curve of recombinant mCherry (1.28-2 µg/ml; BioVision) to extrapolate the mCherry concentration in exo-macs directly from fluorescence intensity values. Both exo-macs and recombinant mCherry were diluted in a buffer containing 30 mM Tris/5 mM CaCl. To specifically degrade free mCherry protein, exo-macs or recombinant mCherry were processed by 1 mM guanidinium hydroxyde (GuOH)/proteinase K (Promega, 0.1 mg/ml) in 30 mM Tris/5 mM CaCl for 2 h at 37°C. To degrade both free and exo-mac-derived mCherry, trichloroacetic acid (TCA 50%, pH = 1) or HCl (0.5M, pH <1) were used.

Quantification of mCherry transfer to acceptor cells

mCherry^{+} exo-macs were purified as described above. iELCs were seeded in 24-well plates, treated with exo-macs (10-20 ng of mCherry equivalents; see above), and allowed to grow for an additional 24 h before analysis. Before immunofluorescence staining, the cells were extensively washed with PBS. Before flow cytometry analysis, the cells were extensively washed with PBS and treated with trypsin/EDTA.

Quantification of miR activity by reporter LVs

Calculation of miR activity

In order to measure endogenous miR activity in live cells transduced with a miRT reporter LV (or no-miRT control LV), we calculated the extent of GFP repression (indicated as "fold repression" or miR activity), as described previously (Brown et al., 2007; Squadrito et al., 2012), by the following equation:

$$\text{miR activity} = (\text{MFI.}\Delta\text{LNGFR}_{\text{miRT}} / \text{MFI.dGFP}_{\text{miRT}}) / (\text{MFI.}\Delta\text{LNGFR}_{\text{no-miRT}} / \text{MFI.dGFP}_{\text{no-miRT}}),$$

where MFI is the mean fluorescence intensity of either GFP or ΔLNGFR measured by flow cytometry, and miRT and no-miRT denote cells transduced with the miRT reporter or control no-miRT LV, respectively.

In order to measure exogenous miR activity in live cells transduced with a miRT reporter LV (or no-miRT control LV) and treated by exo-macs or cocultured with iBMMs, we modified the equation above as follows:

$$\text{miR activity} = ((\text{MFI.}\Delta\text{LNGFR}_{\text{miRT-exo}} / \text{MFI.dGFP}_{\text{miRT-exo}}) / (\text{MFI.}\Delta\text{LNGFR}_{\text{miRT-ctrl}} / \text{MFI.dGFP}_{\text{miRT-ctrl}})) / ((\text{MFI.}\Delta\text{LNGFR}_{\text{no-miRT-exo}} / \text{MFI.dGFP}_{\text{no-miRT-exo}}) / (\text{MFI.}\Delta\text{LNGFR}_{\text{no-miRT-ctrl}} / \text{MFI.dGFP}_{\text{no-miRT-ctrl}})),$$

where “exo” denotes exosome-treated cells, and “ctrl” denotes control, untreated cells.

iBMMs, bENDs, iELCs and Dicer$^{-/-}$ iELCs were seeded in 24-well plates and transduced with individual miRT reporter LVs (or no-miRT control LV), as described above. In most of the experiments, cell transduction was 70–90%, as shown by ΔLNGFR expression by flow cytometry. In some experiments, 1-2 weeks post-transduction the cells were replated in 24-well plates and treated with exo-macs (10 ng of mCherry equivalents). The cells were processed for flow cytometry analysis at 48 h post-exo-mac treatment and miR activity measured as described above.

Matrigel experiment and *in vivo* miR activity studies

Dicer$^{-/-}$ iELCs were seeded in 24-well pates and transduced with the miRT-142-3p reporter LV. One week post-transduction, 2x10^5 *Dicer*$^{-/-}$ iELCs were embedded in matrigel with or without 1x10^6 mCherry$^+$ iBMMs. Matrigel (BD Biosciences) plugs supplemented with 0.5 µg bFGF and 0.5 µg CSF-1 (both from Peprotech) were implanted subcutaneously in the flanks of 8 week-old female swiss *nu/nu* mice. The matrigel implants were harvested 8 days post-injection and processed for flow cytometry analysis.

Flow cytometry

Flow cytometry used a LSR2 apparatus (BD Biosciences). eGFP and mCherry fluorescence were directly analyzed using the 488-525/50 or 561-610/20 nm channels, respectively. Cell suspensions obtained from cultured cells were incubated on ice together with fluorochrome-conjugated antibodies (for a comprehensive list of antibodies, see below), washed and resuspended in PBS with 2% FBS and 7-amino-actinomycin D (7-AAD) to stain nonviable cells. Matrigel implants were excised and made into single-cell suspensions by collagenase IV (0.2 mg/ml, Worthington), dispase (2 mg/ml, Lifetechnologies) and DNaseI (0.1 mg/ml,

New England BioLabs) treatment in IMDM medium. After 30 min at 37°C in a shaking thermoblock, the cell suspensions were filtered and washed in PBS containing 2 mM EDTA and 2% FBS. Matrigel-derived cell suspensions were incubated with rat anti-mouse FcγIII/II receptor (CD16/CD32) blocking antibodies (4 µg/ml), labeled with 7-amino-actinomycin D (7-AAD), and stained with conjugated antibodies.

Immunofluorescence staining and confocal microscopy

Confocal microscopy used a Zeiss LSM 700 Upright confocal microscope coupled to a high sensitivity Axiocam MRm (B/W) camera. Fluorescent signals from the individual fluorophores were sequentially acquired from single optical sections and analyzed and pseudocolored by employing the imaging software ZEN (Zeiss). Cells were seeded on glass Chamber slides (Lab-Tek) coated with 5 µg/cm^2 fibronectin (Roche). At the time of analysis, the medium was aspirated and the cells washed 3 times with PBS, fixed with 4% paraformaldehyde for 15 min, and blocked with 10% normal goat serum (Lifetechnologies) in PBS containing 0.1% Triton X-100 for 30 min. The primary antibodies were then applied for 2-12 h. Slides were washed 3 times and secondary antibodies or phalloïdin (to stain actin) were then applied for 1 h in blocking solution without Triton X-100. After washing, cell nuclei were labelled with DAPI and the slides mounted using FluorSave reagent (Calbiochem). In some experiments, the cells were transduced with a baculovirus expressing a fusion LAMP1/GFP protein to visualize lysosomes. GFP was then acquired by direct fluorescence using the 488 nm channel. In other experiments, a rat anti-mouse LAMP-1 antibody (Abcam) was used to visualize lysosomes.

Antibodies for flow cytometry (FC), immunofluorescence staining (IF), and Western blotting (WB)

Manufacturer	Antigen	Clone	Color	Host	application
BioLegend	F4/80	BM8	APC-Cy7	Rat	FC
BD pharmingen	CD11b	M1/70	FITC	Rat	FC
BioLegend	GR1	RB6-8C5	Pacific Blue	Rat	FC
BD pharmingen	CD31	MEC 13.3	PE	Rat	FC
Miltenyi	dINGFR	ME20.4-1.H4	APC	Human	FC
Abcam	Lamp1	1D4B	na	Rat	IF
Badrilla Ltd.	mCherry	polyclonal	na	Rabbit	IF
AbD Serotec	F4/80	Cl:A3-1	na	Rat	WB
AbD Serotec	CD9	MF1	na	Rat	WB
Abcam	CD11b	polyclonal	na	Rabbit	WB

Sigma	CD81	polyclonal	na	Rabbit	WB
AbD Serotec	Alix	3A9	na	Mouse	WB
R&D	MRC1	polyclonal	na	Goat	WB
Abcam	Calnexin	polyclonal	na	Rabbit	WB
Cell Signalling	Ago2	C34C6	na	Rabbit	WB
Abcam	DCP1A	polyclonal	na	Rabbit	WB
Abcam	GW182	polyclonal	na	Rabbit	WB
Abcam	GAPDH	polyclonal	na	Rabbit	WB
Molecular Probes (Invitrogen)	anti-rabbit		alexa 568	Donkey	IF
Molecular Probes (Invitrogen)	anti-rat		alexa 488	Donkey	IF
GE Healthcare Life Sciences	anti-mouse		HRP	Goat	WB
GE Healthcare Life Sciences	anti-rat		HRP	Goat	WB
Invitrogen	anti-goat		HRP	Rabbit	WB
GE Healthcare Life Sciences	anti-rabbit		HRP	Donkey	WB

Gene expression profiling by individual TaqMan assays

Total RNA was extracted from cells by using the miRNeasy Micro kit (Qiagen), according to the manufacturer's instructions. RNA was quantified using NanoDrop 2000 (Thermoscientific).

miR TaqMan

Reverse transcription (RT) and individual miR profiling were performed using the following miR TaqMan Assays (Life Technologies):

U6, Assay ID: 001973; miR-142-3p, Assay ID: 000464*;* miR-146a-5p, Assay ID: 000468*;* miR-155-5p, Assay ID: 002571*;* miR-15a-5p, Assay ID: 000389*;* miR-16-5p, Assay ID: 000391*;* miR-223-3p, Assay ID: 002295*;* miR-511-3p, Assay ID: 463069_mat*;* let-7a-5p, Assay ID: 000377; miR-218-5p, Assay ID: 00521.

Absolute copy numbers of miR-511-3p were calculated using a standard curve of synthetic miR-511-3p RNA ranging from 6 to $6x10^7$ copies. Dilutions were prepared in 5 ng/µl of yeast RNA (Ambion).

mRNA TaqMan

RNA was retrotranscribed with SuperScript III (Vilo kit, Invitrogen). TaqMan reactions were run for 45 cycles in standard mode using an ABI7900HT apparatus (Applied Biosystems). TaqMan assays used the following probes from Life Technologies:

Arg1, Assay ID: Mm00475988_m1; *Nos2*, Assay ID: Mm00440502_m1, *Hprt*: Assay ID: Mm01545399_m1; *Mrc1*, Assay ID: Mm00485148_m1.

For amplification of *Lyz2*, we used the following custom primers and probe with 5' modification FAM and 3' modification TAMRA (Microsynth).

Fw_Lyz2 primer: CAATGTGCAAAGAGGGTGGTG

Rv_Lyz2 primer: TCGAGGGAATGTGACCTCTCT

Probe: CCGCGGTGTGCTTCTACTGCAGCTC

TaqMan analysis

The SDS 2.2.1 software was used to extract gene expression raw data (C_t). To determine gene expression (for either mRNAs or miRs), we calculated the difference (ΔC_t) between the threshold cycle (C_t) of each gene and that of the reference gene (*Hprt* or *B2m* for mRNAs; U6 or Let7a-5p for miR). The lower the ΔC_t, the higher the gene expression level. In cell fractionation studies, we calculated the ΔC_t using the following formula:

$$\Delta C_t = C_t \text{ (fraction of interest)} - \text{average } C_t \text{ (all fractions)}.$$

Gene expression results are indicated as fold change or relative copies. Fold-changes are calculated using the $2^{-\Delta\Delta Ct}$ method; relative copies using the $2^{-\Delta Ct}$ method, as indicated for each analysis.

Low-density miR TaqMan arrays

Cells

UT and IL-4–treated BMDMs ($10x10^6$ cells from one 10 cm plate) were lysed in Qiazol and RNA extracted and processed as described below. The average yield was 20-50 µg of total RNA for each sample. bEND.3 cells ($2x10^6$ cells from one 10 cm plate) were lysed in Qiazol and RNA extracted and processed as described below. The average yield was 10-20 µg of total RNA for each sample. Coculture of bEND.3 cells with iBMMs was performed using 0.4 µm pore, 24 mm polycarbonate transwell filters (Corning Costar Corp), which allow the free passage of exosomes. iBMMs ($1x10^5$ cells) and bENDs ($2x10^5$ cells) were suspended separately in exosome-free medium supplemented with 50 ng/ml CSF-1 and 50 ng/ml IL-4 (Peprotech). iBMMs were seeded in the upper chamber and bENDs in the lower chamber of the transwell filters. The chambers were then incubated for 48 h at 37°C. bEND.3 cells were

extensively washed in PBS, lysed in Qiazol, and total RNA extracted. The average yield was 10-20 µg of total RNA for each sample.

Exo-macs

The medium conditioned by ~30x10^6 BMDMs or IL-4–treated BMDMs (3-4 10 cm dishes; ~30 ml of medium) was collected after 3 days of culture. The exo-macs were isolated using ExoQuick (as described above) and immediately lysed in Qiazol, and total RNA extracted and processed as described below. The average yield was 500 ng of total RNA for each sample.

RNA processing and TaqMan

We used the Rodent MicroRNA TaqMan Array (Life Technologies) to profile miRs in UT BMDMs; IL-4–treated BMDMs; bEND.3; bEND.3 after coculture with macrophages; exo-macs from UT BMDMs; and exo-macs from IL-4–treated BMDMs. Rodent MicroRNA TaqMan Array comprises cards A (v2.0) and B (v3.0) in a low-density microfluidic 384-well format. Card A contains 384 TaqMan assays enabling the simultaneous quantitation of 329 mouse miRs annotated in miRBase v20. Card B contains 384 TaqMan assays for 289 mouse miRs. Endogenous controls, rat miRs and dead entries are included in each card. In total, 618 unique mouse miRs are profiled. We extracted total RNA (see "*Cells*" and "*Exo-macs*" above) and reverse-transcribed 50 ng of total RNA using Megaplex RT primers (Life Technologies) through a reverse transcription (RT) step that used the TaqMan MicroRNA Reverse Transcription Kit (Life Technologies). The RT products were then preamplified with Megaplex PreAmp Primers (Life Technologies), using the TaqMan PreAmp Master Mix (Life Technologies). We used an Applied Biosystems 7900 HT Real-Time PCR system to run the miR cards. The data were collected and processed using the SDS 2.4 software (Life Technologies) and exported using a detection threshold of 0.1 ΔRn. miRs that had fewer than 2 out of 3 determinations per condition were not considered in the analysis. C_t values were normalized using the Quantile method.

RNA-seq of BMDMs

Sample preparation and sequencing analysis

UT and IL-4–treated BMDMs (10x10^6 cells from one 10 cm plate) were lysed in Qiazol and total RNA extracted. The average yield was 20-50 µg of total RNA for each sample. RNA was DNaseI treated (New England Biolabs) and concentrated using RNAclean XP (Beckman Coulter). RNA was then depleted of rRNA using the Ribo-Zero Magnetic Gold kit (Epicentre Biotechnologies) followed by concentration using RNA Clean & Concentrator -5 columns (Zymo Research). Illumina sequencing libraries were prepared according to the TruSeq RNA

v2 Sample Preparation Guide (Revision B), starting at the RNA fragmentation step. RNA fragmentation with "Elute, Prime, Fragment Mix" was performed for 4 minutes at 94ºC. Sequencing was performed on a HiSeq 2500 (Illumina) using paired-end cBot v3 clustering and TruSeq SBS reagents. Libraries were sequenced using 2 x 100 bp paired-end reads, with 4 indexed samples run per lane, yielding 82-96 million reads (8.2-9.6 Gb) per sample. Image analysis and base calling was performed using Illumina's real time analysis (RTA) software version 1.13.48. Reads were filtered to remove those with low base call quality using Illumina's default chastity criteria. The results were then demultiplexed and converted to fastq format files by CASAVA version 1.8.2. 100 nt paired-end reads from 8 samples (4 IL-4–treated, 4 UT) were then mapped to mm9 reference genome using Tophat software version 2.0.9 (Trapnell et al., 2012), with default options, using mm9 UCSC reference genes GTF (Karolchik et al., 2003). An *ab initio* transcript reconstruction was performed using Cufflinks, version 2.1.1 with default parameters (Trapnell et al., 2012). The resulting GTFs were merged using Cuffmerge, version 2.1.1 (Roberts et al., 2011), using option –g with mm9 UCSC GTF as reference, allowing distinguishing known and novel transcripts. Count data for each exon were generated using htseq-count from the HTseq package (http://www-huber.embl.de/users/anders/HTSeq/, version 0.5.4p3).

Analysis of RNA-seq and TaqMan array data

Differentially expressed gene transcripts (RNA-seq) and mature miRs (TaqMan arrays) were identified using the limma package in R. For gene transcripts, the raw read counts per gene were first filtered for minimal expression (average of raw counts >5 across samples), normalized to the relative size of each library using the R package edgeR, and then transformed to log2-cpm (counts per million reads) using the voom function. Empirical Bayes moderated t statistics and corresponding p-values were then computed for the comparison (IL-4–treated vs UT). p values were adjusted for multiple comparisons using the Benjamini Hochberg procedure (Benjamini and Hochberg, 1995). Gene transcripts and miRs with an adjusted p value of ≤0.05 were considered to be differentially expressed.

Fragments per kilobase per million of reads (FPKM) were estimated for transcripts in each of the conditions using the cufflinks software (version 2.1.1). Option -G was used, together with the UCSC transcripts reference. Other options were default.

Hierarchical clustering

The heatmaps were generated using heatmap.2 from the package gplots in R, version 2.11.0 (Warnes et al.). The clustering was performed using hclust, version 1.3. (Warnes et al.), using Spearman correlation and euclidean (for RNA-seq analysis) and ward (for TaqMan array analysis) average linkage clustering. A scaling by row was applied.

Correlation analysis

To test the hypothesis that IL-4–induced changes in exo-miR levels were dependent on quantitative changes in miR target levels in the BMDMs, we implemented a computational model in R. We considered the following variables:

(i) The $\log_2$ fold-change (FC) values representing miR increase/decrease in exo-macs vs BMDMs by IL-4.

Log_2FC values (exo-macs vs BMDMs; IL-4–treated vs UT) were calculated in R by using the Limma package by implementing the following contrast: (exo-mac_IL4 – exo-mac) – (BMDM_IL4 – BMDM).

(ii) The ln of the weighted interaction score (WIS) ratio (WIS-ratio) or the Δ-WIS, both representing IL-4–induced changes in the abundance of miR:target interactions.

For each miR (*m*), the WIS is defined as the total number of weighted interactions with all predicted targeted transcripts (*t*). The WIS is therefore calculated by considering (i) the absolute expression of each transcript (*t*); (ii) the number of predicted binding sites in the 3'-UTR of each transcript (*t*); (iii) the strength of the miR:target interaction for each site.

For each miR (*m*), the ln(WIS-ratio) and the Δ-WIS are calculated by comparing the WIS of IL-4–treated vs UT BMDMs, as follows:

$$\ln(\text{WISratio}_{(m)}) = \ln(\text{WIS}_{IL4(m)} / \text{WIS}_{UT(m)})$$

$$\Delta\text{-WIS} = \text{WIS}_{IL4(m)} - \text{WIS}_{UT(m)}$$

where $\text{WIS}_{IL4(m)}$ and $\text{WIS}_{UT(m)}$ represent the WIS values for a given miR in IL-4–treated and UT BMDMs, respectively. WIS values for each miR ($\text{WIS}_{(m)}$) consider the weighted sum of all predicted miR:target interactions using the following equation:

$$\text{WIS}_{(m)} = (S_{6mer(m)} * w_{6mer}) + (S_{7mer(m)} * w_{7mer}) + (S_{8mer(m)} * w_{8mer})$$

The variables $S_{6mer(m)}$, $S_{7mer(m)}$ *or* $S_{8mer(m)}$ represent the total number of predicted 6, 7 or 8mer targets for each miR (*m*) and are calculated by computing (i) the absolute expression level of each transcript (*t*) and (ii) the number of predicted target sites in the 3'-UTR of each transcript (*t*), using the following equation:

$$S_{6mer(m)} = F_{FPKM(t1)} * T_{6mer(t1)(m)} + F_{FPKM(t2)} * T_{6mer(t2)(m)} + [\ldots] + F_{FPKM(tN)} * T_{6mer(tN)(m)}$$

$$S_{7mer(m)} = F_{FPKM(t1)} * T_{7mer(t1)(m)} + F_{FPKM(t2)} * T_{7mer(t2)(m)} + [\ldots] + F_{FPKM(tN)} * T_{7mer(tN)(m)}$$

$$S_{8mer(m)} = F_{FPKM(t1)} * T_{8mer(t1)(m)} + F_{FPKM(t2)} * T_{8mer(t2)(m)} + [\ldots] + F_{FPKM(tN)} * T_{8mer(tN)(m)}$$

where $F_{FPKM(t)}$ is the FPKM value for a transcript (*t*), and $T_{6mer(t)(m)}$, $T_{7mer(t)(m)}$ *and* $T_{8mer(t)(m)}$ are the numbers of 6, 7 and 8mer miR-seed:target interactions for the miR *(m)* in the 3'-UTR of the transcript (*t)*. Sequences involved in miR-seed:target interactions in the transcripts were classified as follows:

1. 6mer: sequence complementary to position 2 to 7 of the miR, corresponding to 6merβ miR-seed:target interactions, as defined by (Ellwanger et al., 2011). This category also includes approximately 75% of all 7merA1 miR-seed:target interactions, as defined by (Grimson et al., 2007).
2. 7mer: sequence complementary to either position 1 to 7 or 2 to 8 of the miR. The sequence complementary to position 1 to 7 corresponds to 7merα miR-seed:target interactions, as defined by (Ellwanger et al., 2011) and also includes approximately 25% of all 7merA1 miR-seed:target interactions, as defined by (Grimson et al., 2007). The sequence complementary to position 2 to 8 includes the 7merβ, miR-seed:target interactions, as defined by (Ellwanger et al., 2011), which corresponds to the 7mer-m8, miR-seed:target interactions, as defined by (Grimson et al., 2007). This category also includes approximately 75% of all 8merA1 miR-seed:target interactions, as defined by (Grimson et al., 2007).
3. 8mer: sequence complementary to position 1 to 8 of the miR, corresponding to 8merα miR-seed:target interactions, as defined by (Ellwanger et al., 2011). This category also includes approximately 25% of all 8merA1 miR-seed:target interactions, as defined by (Grimson et al., 2007).

The aforementioned miR-seed:target interactions were then identified in the 3'-UTR of all transcripts using the vcountPattern function contained in the Biostring package, using R (Pages et al.). The 3'-UTR sequences of 46982 transcripts were retrieved from UCSC, mm9. The parameters w_{6mer}, w_{7mer} *and* w_{8mer} represent the values 0.3, 0.7 and 1.0, respectively, which we implemented in the formula to adjust (weight, *W*) the contribution of each type of miR-seed:target interaction to the WIS value based on the predicted affinity of each seed type to the target RNA. The values 0.3, 0.7 and 1.0 were selected based on published reports that investigated the strength of the different miR-seed:target interactions using miR transfection experiments and mRNA microarray analysis (Ellwanger et al., 2011; Grimson et al., 2007).

The correlation between ln(WIS-ratio) and $\log_2$FC was validated using the following resampling techniques:

(i) Bootstrap by permuting the values 10'000 times and calculating an empirical p value (bootstrap p value) measuring how often the correlation is observed by chance.

(ii) Measuring the robustness of the correlation by excluding 5, 10 and 20% of the points and re-calculating the correlation 10'000 times to assess how the correlation is impacted.

Removing in silico the contribution of targeted transcripts from the WIS

We first calculated the WIS of individual transcripts (*t*) for each miR (*m*) in both IL-4–treated (*t.IL4*) and UT (*t.UT*) BMDMs, using a modified version of the equation described above, as follows:

$$WIS_{(t.IL4)(m)}=w_{6mer}*F_{FPKM(t.IL4)}*T_{6mer(t)(m)} + w_{7mer}*F_{FPKM(t.IL4)}*T_{7mer(t)(m)} + w_{8mer}*F_{FPKM(t.IL4)}*T_{8mer(t)(m)}$$
$$WIS_{(t.UT)(m)}=w_{6mer}*F_{FPKM(t.UT)}*T_{6mer(t)(m)} + w_{7mer}*F_{FPKM(t.UT)}*T_{7mer(t)(m)} + w_{8mer}*F_{FPKM(t.UT)}*T_{8mer(t)(m)}$$

We then calculated the difference *(Δ)* between the WIS of the transcript *(t)* in IL-4–treated and UT BMDMs. *(Δ)* measures the absolute contribution of the transcript (*t)* to the WIS in IL-4–treated vs UT BMDMs:

$$\Delta_{(t)(m)} = \left| WIS_{(t.IL4)(m)} - WIS_{(t.UT)(m)} \right|$$

We ranked, for each miR *(m)*, N transcripts *(t)* according to their Δ values (from highest to lowest; decreasing contribution to the WIS). We then measured the increase/decrease of the WIS ($WIS_{(-tN)(m)}$) by removing from the WIS of IL-4–treated BMDMs ($WIS_{(m)IL4}$) the Δ of each transcript ($\Delta_{(tN)}$), one by one and cumulatively, as follows:

$$WIS_{(-t1)(m)} = WIS_{(m)IL4} - \Delta_{(t1)(m)}$$
$$WIS_{(-t1-2)(m)} = WIS_{(m)IL4} - \Delta_{(t1)(m)} - \Delta_{(t2)(m)}$$
$$WIS_{(-t1-3)(m)} = WIS_{(m)IL4} - \Delta_{(t1)(m)} - \Delta_{(t2)(m)} - \Delta_{(t3)(m)}$$
$$[\ldots]$$
$$WIS_{(-t1-N)(m)} = WIS_{(m)IL4} - \Delta_{(t1)(m)} - [\ldots] - \Delta_{(tN)(m)}$$

Finally, we calculated the percentage of the $WIS_{(-t1-N)(m)}$ compared to the $WIS_{(m)IL4}$, as follows:

$$\% \text{ of WIS} = 100 * WIS_{(m)IL4} / WIS_{(-t1-N)(m)}$$

Difference of FC (enrichment in exo-macs by IL-4) between miRs belonging to the same miR family

We first created 4 groups of miR pairs according to the similarity of their sequences:

group 1: all the miR pairs sharing the same sequence from position 2 to 8;

group 2: all miR pairs sharing 3mer sequences in the same position (9 to 17) of their sequence. This group contains 10 subgroups based on the position of the 3mer sequence;

group 3: all miR pairs sharing 4mer sequences in the same position (9 to 16) of their sequence. This group contains 9 subgroups;

group 4: all possible miRNA pairs. In this case, we identified 15'753 miR pairs (for all the 178 miRs analyzed).

We then calculated the *difference* between the FC of the 2 miRs in each miR pair, as follows:

$$difference = (log_2(FC.miR1) - log_2(FC.miR2))^2$$

FC represents the miR fold-change in exo-macs vs BMDMs induced by IL-4 (FCs for individual miRs are showed in Table S2E). The resulting values are shown by cumulative curves, each representing a different group/subgroup. Statistical analysis was performed by comparing group 4 with groups 1-3.

Statistical analysis

Statistical analysis of the data is described in the figure legends. Error bars show standard error of the mean (SEM), unless stated otherwise. Statistical significance of the data is indicated as follows: *: $p < 0.05$; **: $p < 0.01$; ***: $p < 0.001$.

Supplemental References

Benjamini, Y., and Hochberg, Y. (1995). Controlling the False Discovery Rate: A Practical and Powerful Approach to Multiple Testing. J. R. Stat. Soc. Series B Stat. Methodol. *57*, 289-300.

Cobb, B.S., Nesterova, T.B., Thompson, E., Hertweck, A., O'Connor, E., Godwin, J., Wilson, C.B., Brockdorff, N., Fisher, A.G., Smale, S.T.*, et al.* (2005). T cell lineage choice and differentiation in the absence of the RNase III enzyme Dicer. J. Exp. Med. *201*, 1367-1373.

De Palma, M., Mazzieri, R., Politi, L.S., Pucci, F., Zonari, E., Sitia, G., Mazzoleni, S., Moi, D., Venneri, M.A., Indraccolo, S.*, et al.* (2008). Tumor-targeted interferon-alpha delivery by Tie2-expressing monocytes inhibits tumor growth and metastasis. Cancer Cell *14*, 299-311.

De Palma, M., and Naldini, L. (2002). Transduction of a gene expression cassette using advanced generation lentiviral vectors. Methods Enzymol. *346*, 514-529.

Karolchik, D., Baertsch, R., Diekhans, M., Furey, T.S., Hinrichs, A., Lu, Y.T., Roskin, K.M., Schwartz, M., Sugnet, C.W., Thomas, D.J.*, et al.* (2003). The UCSC Genome Browser Database. Nucleic Acids Res. *31*, 51-54.

Pages, H., Aboyoun, P., Gentleman, R., and DebRoy, S. Biostrings: String objects representing biological sequences, and matching algorithms.

Roberts, A., Pimentel, H., Trapnell, C., and Pachter, L. (2011). Identification of novel transcripts in annotated genomes using RNA-Seq. Bioinformatics *27*, 2325-2329.

Trapnell, C., Roberts, A., Goff, L., Pertea, G., Kim, D., Kelley, D.R., Pimentel, H., Salzberg, S.L., Rinn, J.L., and Pachter, L. (2012). Differential gene and transcript expression analysis of RNA-seq experiments with TopHat and Cufflinks. Nat. Protoc. *7*, 562-578.

Warnes, G., Bolker, B., and Lumley, T. gplots: Various R programming tools for plotting data. R package version 2.6.0.

Xia, W., Zhang, J., Ostaszewski, B.L., Kimberly, W.T., Seubert, P., Koo, E.H., Shen, J., and Selkoe, D.J. (1998). Presenilin 1 regulates the processing of beta-amyloid precursor protein C-terminal fragments and the generation of amyloid beta-protein in endoplasmic reticulum and Golgi. Biochemistry *37*, 16465-16471.